Cement and Concrete Composites 141 (2023) 105121

Contents lists available at ScienceDirect

Cement and Concrete Composites

journal homepage: www.elsevier.com/locate/cemconcomp

Effect of proteins on the mineralization, microstructure and mechanical properties of carbonation cured calcium silicate

Elvis Baffoe, Ali Ghahremaninezhad *

Department of Civil and Architectural Engineering, University of Miami, Coral Gables, FL, 33146, United States

ARTICLE INFO

Keywords:
Wollastonite
Proteins
Carbonated curing
Microstructure
Cracks

ABSTRACT

The effect of five proteins with different physicochemical properties on the mineralization, microstructure, and mechanical properties of carbonated wollastonite pastes was examined. The negative surface charge of wollastonite particles increased as the result of protein adsorption. The flow of fresh paste was shown to increase in the pastes with proteins due to the enhanced electrostatic repulsion of the wollastonite particles as a result of the adsorption of negatively charged proteins, the ball bearing effect of the proteins in the pore solution, and formation of air bubbles. While calcite and amorphous calcium carbonate were the primary phases of calcium carbonate in all pastes, other polymorphs including aragonite and vaterite were present, to a small extent, in the microstructure of most of the pastes modified with proteins. The calcium carbonate content was shown to be higher in some of the pastes modified with proteins and this was attributed to the delayed water loss to evaporation and presence of free water due to hydrophobization of pastes modified with proteins. The X-ray micro-computed tomography (micro-CT) analysis revealed the formation of cracks in the control and some of the protein modified pastes resulting from drying shrinkage. It was demonstrated that the increased microstructure hydrophobicity was the reason for the absence of cracks in the pastes with the proteins that did not show cracks. Overall, the carbonated pastes with proteins exhibited higher compressive strength compared to the control paste. Absence of cracks, enhanced interfacial strength between carbonated products in the microstructure and organic-inorganic composite formation are suggested to be responsible for the increased compressive strength of the carbonated pastes with proteins.

1. Introduction

There has been an increasing interest in the development of alternative binder materials for construction applications. This is particularly because the production of ordinary Portland cement (OPC) which is an important component of concrete materials contributes to about 5% of the global anthropogenic carbon dioxide (CO_2) emissions [1]. In addition, due to an extensive energy required in manufacturing OPC, the OPC production accounts for about 5% of the total industrial energy consumption worldwide [1,2], thus making it a global concern. In order to address the environmental concerns related to use of OPC, the utilization of alternative binder materials with low carbon footprint and less energy input towards their production has gained increasing interest in recent decades [3–9].

Wollastonite is one of such alternative binders which has gained attention in recent years [10–13]. Wollastonite is a non-hydraulic calcium silicate ($CaSiO_3$) binder, which is activated by reacting with CO_2 in the presence of moisture to form calcium modified silica gel and calcium carbonate ($CaCO_3$) [14]. This process of activation was first reported in the 1990s [15] and it is primarily used for the activation of calcium silicate bearing minerals. Just like the calcium-silicate-hydrate (*C*–S–H) phase in hydraulic cement, these carbonation reaction products (Ca-modified silica gel and $CaCO_3$) act as binders and are responsible for strength development in wollastonite paste [16]. The carbonated wollastonite binder material has exhibited performance similar to or higher than that of OPC in aggressive conditions [17].

Prior investigations examined the mechanical performance of mortar specimens manufactured using wollastonite as the sole binder phase and reported a higher compressive strength as high as 35 MPa after the paste had been subjected to carbonation curing for 1140 min [14]. In another study, Ashraf et al. [16] examined the strength development of calcium silicates and reported a compressive strength of 37 MPa after 140 h of carbonation period. The strength development of these carbonated pastes has been determined to be largely attributed to the formation of

* Corresponding author.
E-mail address: a.ghahremani@miami.edu (A. Ghahremaninezhad).

https://doi.org/10.1016/j.cemconcomp.2023.105121
Received 6 December 2022; Received in revised form 17 April 2023; Accepted 3 May 2023
Available online 3 May 2023

$CaCO_3$ [18]. The compressive strength of the carbonated matrix has been noted to increase with increasing carbonation curing period and this has been shown in the thermogravimetric analysis (TGA), X-ray diffraction (XRD) and Fourier transform infrared spectrometry (FTIR) measurements that, as carbonation progresses the peaks associated to calcium silicates reduce while $CaCO_3$ peaks increase [16]. The $CaCO_3$ binding phase is first formed in smaller capillary pores as amorphous calcium carbonate (ACC) or microcrystalline phase [19]. The amorphous phases undergo nucleation, growth and transition into vaterite or aragonite and finally into crystalline calcite which eventually seal large pores to reduce permeability of the composite [3,19].

Inspired by nature, efforts have been made to use biomolecules to fine tune the structure of $CaCO_3$ at the nano and microscales so as to enhance the performance at the macroscale [20]. This may allow the production of low CO_2 footprint binders with higher mechanical and durability properties. Several studies have reported the influence of biomolecules on the morphological and mechanical properties of $CaCO_3$ [7,21–24]. For instance, Polowczyk et al. [22] investigated the effect of ovalbumin and lysozyme on the morphology of $CaCO_3$ and observed 'stack-like' structures in the albumin modified $CaCO_3$. They attributed the morphological changes to the electrostatic interaction between the negatively charged ovalbumin and Ca^{2+} which leads to the coalescence and creation of a steric barrier preventing the growth of particles. Yang et al. [23] studied the interaction of bovine serum albumin (BSA) with $CaCO_3$ synthesized through gas-diffused method and reported the formation of $CaCO_3$ with hierarchical structures. The authors attributed this observation to the binding interactions between BSA and $CaCO_3$. Kim et al. [24] investigated the interaction between two sets of amino acids and calcite. The findings by the authors revealed the formation of organic-inorganic composites with outstanding mechanical properties comparable to biological composites. Despite a significant number of studies on the use of biomolecules to modulate the morphology and mechanical properties of $CaCO_3$, investigations on the use of biomolecules in CO_2 activated binders are lacking. To the best of our knowledge only Khan et al. [7] utilized amino acids to modify the performance of a CO_2 activated binder. Nonetheless, the work by Khan et al. [7] was mostly focused on the polymorph and mechanical performance of carbonated wollastonite paste with and without amino acids. The present study is carefully designed to increase the knowledge about the effect of proteins on carbonated wollastonite binder. Proteins are forms of biomolecules consisting of different amino acids that are joined together by peptide bonds [25]. Amino acids are the building block of proteins and may be non-polar hydrophobic, polar hydrophilic, basic and acidic in nature providing an assembly of interaction pathways between their side chains and other solid surfaces [25]. Considering the charge variations of the proteins, they may interact with cementitious materials which are equally heterogeneous [26].

In the present study, the influence of proteins with different molecular structures on the mineralization of $CaCO_3$ formed as a result of wollastonite carbonation was studied and evaluated through FTIR, TGA, XRD, and Scanning Electron Microscopy (SEM). The X-ray micro-computed tomography (micro-CT) was employed to examine the internal structure and drying shrinkage of the carbonated wollastonite paste. The physicochemical properties of the proteins including zeta potential, surface adsorption, surface tension, in the wollastonite environment as well as their effect on pore surface hydrophobization, were assessed. The compressive strength of the carbonated wollastonite was evaluated and discussed.

2. Experiments

2.1. Materials

Wollastonite powder (Calcium metasilicate) is obtained from Seaforth Mineral and Ore Co., INC USA. The oxide composition of the wollastonite powder evaluated using X-ray Fluorescence (XRF) is presented in Table 1. The specific surface area and mean particle size of the wollastonite powder is 1.8 m^2/g and 9 μm, respectively. Five proteins with different molecular structures, namely, (ovalbumin) albumin, collagen peptide (CP), whey protein, non-fat milk powder (NFMP) and sodium immunoglobulin (SBI) were purchased and used in this study. In their respective native states, whey protein, albumin, NFMP, and SBI are reported to be globular in shape while CP is fibrous in their native state [27–29]. SBI consists of approximately 90% protein and can be obtained by fractionating edible grade bovine plasma [30]. NFMP consists of about 80% casein proteins [31]. The albumin utilized in the experiment consists of about 54–58% by weight of the egg white protein [32]. Whey protein concentrate can be obtained as a by-product of cheese making process [27]. Collagen on the other hand is a structural protein with high content of hydroxyproline and proline [25]. The molecular structures of these proteins have been studied in a previous study [33].

2.2. Sample preparation and carbonation of wollastonite pastes

Wollastonite paste was prepared by hand-mixing wollastonite powder with deionized water at a water to wollastonite ratio of 0.45 for 3 min. For the paste containing proteins, proteins at the concentrations of 0.25% and 1%, per wollastonite mass, were mixed with deionized water and stirred continuously for 10 min. After 10 min of continuous stirring, the protein solution was hand-mixed with the wollastonite powder for an additional 3 min. The mixed pastes (both the control and the protein modified ones) were spread on a thin glass slide with the dimensions of 25 mm × 1 mm × 75 mm. Care was taken to ensure that the thickness of the wollastonite paste was approximately 2 mm. The small paste thickness was to ensure uniform carbonation of the pastes. In addition, the paste was not tamped to avoid possible diffusion of CO_2 even before the pastes were subjected to carbonation. Right after this process, the pastes were clearly labelled and placed inside a water-jacketed CO_2 chamber designed and manufactured by Lab-Line for the carbonation curing process.

The condition of the carbonation process was set at a relative humidity (RH) of 95% at a temperature of 55 °C. The carbonation flow rate was set at 8 cubic feet per hour; thus, a timer was set to bring the level of CO_2 up to 20% and then shut down until after 12 h where the process was repeated again. The flow rate for CO_2 was set based on the dimensions of the CO_2 chamber. The pastes were kept inside the carbonation chamber for different durations of 8 h, 18 h, 72 h, 168 h, and 336 h before testing. The microstructural and chemical characterization of the thin paste carbonated pastes were evaluated using FTIR, TGA, XRD and SEM.

Cube wollastonite pastes with the same mix design as in the thin paste samples were prepared and used in the contact angle test, compressive strength test and micro-CT analyses. In addition, in order to examine the effect of sample size, the samples obtained from the core of the cubes were also studied using TGA, FTIR, and SEM. The wollastonite paste was cast in a prismatic metallic molds with dimensions of 25 mm × 25 mm × 300 mm and compacted with a tamper for 2 min to achieve a uniform compaction level. The compacted pastes were placed inside the CO_2 chamber with the same condition described previously, except that CO_2 inside the chamber was refilled after every 8 h to ensure maximum degree of carbonation. The pastes were then demolded after 48 h of carbonation curing and placed back inside the carbonation chamber for the carbonation process to continue. On the 10th and 25th day, the prismatic pastes were cut into 25 mm × 25 mm × 25 mm cubes using a wet diamond saw. The pastes were again put inside the CO_2 rich incubator after cutting and then tested the following day.

Table 1
Oxide composition of raw wollastonite in this study.

Oxide	SiO_2	CaO	Al_2O_3	MgO	Fe_2O_3	LOI
%	51.3	44.9	0.9	1.6	<0.2	1.1

2.3. Methods

2.3.1. Zeta potential

The zeta potential of the protein solution adjusted to the pH level of 8.8 and wollastonite suspension were determined using dynamic light scattering in a Zetasizer Nano ZS instrument (Malvern Instruments Ltd., Malvern, U.K.) conditioned at 25 °C. The pH of the protein solution was adjusted to 8.8 because that was the pH of the wollastonite suspension. Wollastonite pastes with a water to wollastonite ratio of 1 and with and without proteins were prepared. The concentration of the protein used was 0.15% by mass of deionized water. After mixing the pastes for 3 min, the paste was centrifuged at 500 rpm for 5 min to collect the suspension. The suspension was filtered by a vacuum pump fitted with a 0.8 μm filter paper and then equilibrated for 10 min. After 10 min of equilibration, the suspension was filled in a disposable folded capillary cell (DTS1070) and loaded into the instrument. After loading into the device, the samples were equilibrated for 120 s before testing. Each sample was tested three times and in between each test, data was collected after 100 or 110 runs. The same protocol was followed to determine the zeta potential of the protein solution adjusted to pH level 8.8, except that these samples were not centrifuged since they did not contain any solid particles. The zeta potential parameters, namely, refractive index (RI) and absorption for the proteins were set at 1.45 and 0.001, respectively.

2.3.2. Surface adsorption

The concentration of the proteins adsorbed on wollastonite particle surface was measured using the Agilent 8453 UV–Vis spectrophotometer at 25 °C based on the difference in absorbance intensity. The test was done at the wavelength of 562 nm which is suitable for protein quantification analysis using the Bradford protein assay (BCA) [34,35]. For sample preparation, 0.4 mL of deionized water was mixed with 0.5 g of wollastonite and left to stand for 20 min to allow the dissolution of the various ions present in the paste. After 20 min, 0.1 mL of each prepared protein solution was mixed with the wollastonite paste mixture and ultra-sonicated for 25 min. Another 0.1 mL of each protein concentration was mixed with 0.4 mL deionized water to serve as the standard protein concentration in μg/ml. The concentrations of the prepared protein solutions were 3000 μg/ml, 2000 μg/ml, 1000 μg/ml, 800 μg/ml and 500 μg/ml.

The wollastonite paste mixture with protein after the ultrasonication process was centrifuged for 10 min. Approximately 0.1 mL of the supernatant was mixed with 2 mL of BCA reagent and incubated in an oven for 30 min at 37 °C. Similarly, 0.1 mL of original protein concentration was mixed with 2 mL of the BCA reagents and incubated for the same period and incubation conditions. After the incubation period, the mixture was cooled for 10 min at room temperature and absorbance values of the mixtures recorded. A purple color indicates the presence of protein in the solution [35]. The Standard (original) protein concentrations were plotted against their respective absorbance values and a linear equation generated. Then, the absorbance of the proteins in the supernatant was measured. By using the linear equation generated from the standard curve (original concentration versus their respective absorbance values) and the absorbance value of the protein in the supernatant, the concentration of protein in the supernatant was determined. The concentration of the protein adsorbed on the wollastonite paste was determined from the difference between the concentration of the protein in the equivalent volume of deionized water only and the concentration of the supernatant.

2.3.3. Flow test

The influence of the proteins on the flowability of the wollastonite paste was measured using a mini slump test. Wollastonite pastes with a water to wollastonite ratio of 0.45 and with protein concentrations of 0%, 0.25%, 0.5%, and 1%, per mass of wollastonite powder, were mixed in a rotary mixer for 5 min. Then, the freshly prepared pastes were allowed to rest inside the mixing container while covered for 5 min. Then, the pastes were filled inside a Vicat cone and placed at the center of a tray. The cone had a top diameter of 75 mm, a bottom diameter of 100 mm, and a height of 50 mm. The paste was allowed to rest inside the cone for 1 min. Then, the cone was removed, and the tray was gently dropped on a table 25 times with a consistent rate over a period of 10 s. The average of two perpendicular diameters of the spread was measured as the flow value. Three replicates were used for each mix design.

2.3.4. Surface tension

The surface tension of the pore solution of the wollastonite pastes with and without proteins was measured with the KRŮSS Digital Tensiometer K10S using the ring method.

Pastes with water to wollastonite ratio of 0.45 and with protein concentrations of 0%, 0.25%, 1%, and 2%, per wollastonite mass, were mixed, sealed, and allowed to rest for 20 min.

After 20 min, the pastes were centrifuged at 4500 rpm for 5 min to collect the pore solution. The extracted solution was filtered by a vacuum pump fitted with a 0.8 μm filter paper. The filtered solution was collected inside a ring and analyzed using the surface tensional analyzer. The diameter and thickness of the ring was 9.36 mm and 0.37 mm, respectively. Before each run, the ring was thoroughly heated by a wick flame and cleaned with acetone to remove organic contaminants. Three replicates were tested for each sample and the average reported.

2.3.5. Water contact angle

The water contact angle between deionized water and carbonated wollastonite paste was measured by a simple apparatus comprising a dropper and a camera of higher resolution. Carbonated wollastonite paste cubes of dimensions 25 mm × 25 mm × 25 mm were used for the measurement. The surface of the carbonated paste cubes cured for 11 and 26 days was polished using SiC sandpapers with grit numbers of 320, 500, and 1200, and finely polished with a 1 μm diamond abrasive. The polished pastes were vacuum dried at 50 °C for 24 h. About 5 μL of deionized water droplet was cast on the surface of the carbonated paste. Images of the shape of the stable deionized water droplets on the surface were taken using a high-resolution camera. The angle between the surface of the droplet and the surface of the carbonated paste was measured using the image J software. The average of approximately 20 different contact angle measurements per each mix design was calculated and reported.

2.3.6. FTIR

FTIR was employed to investigate the chemical phases in the carbonated thin pastes and in the core of the carbonated cube pastes cured for different durations. These pastes were ground into fine powder and passed through sieve # 60. Approximately, 30 mg of ground carbonated paste was utilized for the test. The FTIR measurements were performed using a PerkinElmer Paragon 1000 FTIR with an ATR accessory in the transmission mode. The scans were taken at the resolution of 4 cm^{-1} and between 600 cm^{-1} and 4000 cm^{-1}. Each sample was taken through 4 scans and the average of two scans from the 4 rounds of scans was reported.

2.3.7. TGA

TGA was employed to investigate the mineralogical composition of the carbonated thin pastes and in the core of the carbonated cube pastes cured for different durations. The sample preparation was the same as described for the FTIR test. Approximately 50 mg was loaded into the TGA pan. The samples were scanned using the Netzsch TG at a heating rate of 20 °C/min and in the temperature range of 24 °C to 900 °C. Two replicates of each sample were used, and the average reported.

2.3.8. XRD

The chemical characteristics of the carbonated thin pastes were studied using a Rikagu X-ray Diffractometer (Model D/Max-3C, Rikagu,

Japan). The XRD scans were taken using a Cu Kα radiation (40 kV, 20 mA), with a scan interval of 2 θ = 10° to 40°, and a step size of 0.02°. Sample preparation was the same as described for the FTIR test. Approximately 2 g of the ground paste was loaded into a sample holder and inserted into the device. The Rietveld refinement was carried out to compare the relative proportions of the crystalline phases with a Match! Phase Analysis using Powder Diffraction software.

2.3.9. SEM

The SEM images of the carbonated pastes were obtained using a Zeiss Gemini Ultra Plus FESEM in the secondary electron mode. For sample preparation, the 168-h carbonated thin pastes formed on glass slides were ground into powder, passed through the sieve # 60 and gold coated. The fractured surfaces of the cube pastes used in the compressive strength test were also gold coated and investigated using the SEM. These pastes were modified with 1% protein concentration and carbonated for 26 days prior to testing.

The gold coating was to decrease the effect of charging at higher kV and magnification. The accelerating voltage was 10.00 kV, and the working distance (WD) was 5 mm. Images were taken at the magnification of 10000X.

2.3.10. X-ray micro-CT and drying shrinkage measurement

The internal structure of the carbonated cube pastes with and without proteins was evaluated using the Bruker SkyScan 1273 micro-CT at a resolution of 14 μm/pixel. The pastes used were the 26-day carbonated cube pastes. The rotational step, exposure time, voltage and current were 0.6°, 4350 ms, 130 kV and 115 μA, respectively. The pastes were placed on a bronze stand and positioned between an X-ray source and an X-ray detector and scanned for a period of approximately 6 h during which about 345 projections over 180° were taken. The scanned pastes were quantitatively analyzed using CTAnalyzer 1.20.8. The 2 D reconstructed sections, void volume distribution, total porosity, volume fraction of cracks, and average void size in the internal structure of the pastes were quantified. The sphericity was used to distinguish the microcracks from voids. Sphericity values ranged between '0' and '1' where '1' is regarded as perfect spheres. For the purpose of this analysis, spherical values equal to or less than 0.1 were marked as microcracks. The dimensional change of the 26-day carbonated pastes with and without proteins was measured using the 2D slices obtained from the reconstructed images. The areal shrinkage (% mm^2/mm^2) of 20 cross sections of each sample was measured using the image J software and the average was reported.

2.3.11. Compressive strength

The compressive strength of the carbonated wollastonite cube pastes with and without proteins was measured after 11 and 26 days of carbonation curing. The compressive strength test was performed using a SATEC testing machine at a loading rate of 0.05 mm/s. Five replicates of each mix design were tested, and the average reported. Another batch of cubes was used to assess their durability in a wet environment. To this end, the 1% protein modified cubes after 26 days of carbonation were submerged in deionized water for 24 h and then their compressive strength was measured.

3. Results and discussions

3.1. Physiochemical properties

3.1.1. Zeta potential

Fig. 1 shows the zeta potential of the proteins in NaOH solution at pH = 8.8 and the zeta potential of the wollastonite suspension containing proteins. A general negative zeta potential value of the proteins at the pH level of 8.8 is observed and this is attributed to the deprotonation of the amino acid functional groups of the proteins at the pH level of 8.8 [31,36,37]. The zeta potential value of the wollastonite

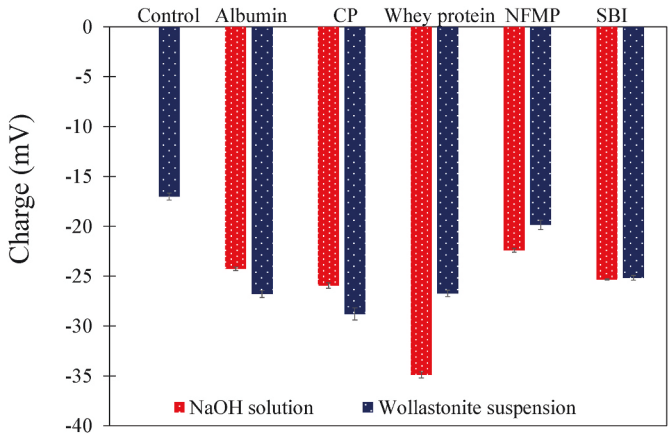

Fig. 1. Influence of admixed proteins on the zeta potential of NaOH solution at pH level 8.8 and wollastonite suspension.

suspension was approximately −17 mV and that was mainly attributed to the presence of silicate groups on the surface of wollastonite particles [38]. A similar zeta potential value of wollastonite suspension was reported by Kangal et al. [38].

The mineralogical composition of wollastonite is mainly made up of SiO_2 and CaO as revealed in Table 1 and reported by Kangal et al. [38]. Ca^{2+} dissolved from wollastonite into the solution can adsorb onto the negatively charged silicates on the surface rendering a portion of the wollastonite surface positively charged. However, the net surface charge of the wollastonite particles remains negative as evidenced in Fig. 1. It is noticed that the negative surface charge of wollastonite particles increases when the proteins are added to the suspension. This could be a result of the adsorption of negatively charged proteins onto the negatively charged wollastonite particles through Ca^{2+} bridging, thus further increasing the negative surface charge density.

Furthermore, the interaction between the negatively charged segments of the proteins and the Ca^{2+} ions released into the solution [39] could result in the chelation of Ca^{2+} with proteins, which reduces the concentration of Ca^{2+} in the solution, and subsequently, diminishes the positively charge portion of the wollastonite surface covered by Ca^{2+}. It is noted that wollastonite particles with NFMP exhibited the lowest surface charge compared to wollastonite particles with other proteins; also, NFMP had the lowest surface charge among the proteins studied here. The aggregation of the charged amino acids in the molecular structure of individual proteins in a certain condition sums up the overall surface charge of the proteins [31,40]. The low surface charge of NFMP compared to other proteins could be due to a lower combined charge of the charged amino acids in the make-up of NFMP corresponding to the pH of the solution. The variability in surface charge of the wollastonite with proteins indicates the contribution of protein adsorption on the change in surface charge of wollastonite particles.

3.1.2. Surface adsorption

The adsorption of the proteins onto the surface of wollastonite particles as measured by UV–Vis spectrophotometry is shown in Fig. 2. Generally, it can be seen that the proteins showed moderate affinity to wollastonite particles and the adsorption values are seen to increase with increasing protein concentration as the adsorption site on the wollastonite particles surfaces have not been fully occupied by the proteins. As discussed previously, electrostatic interaction can be hypothesized to be one of the mechanisms driving the adsorption of the negatively charged proteins onto negatively charged wollastonite particles via Ca^{2+} bridging.

In addition to the electrostatic interactions, since the molecular structure of the proteins consists of various functional groups with the ability to interact via hydrogen bond formation – hydroxyl or amide

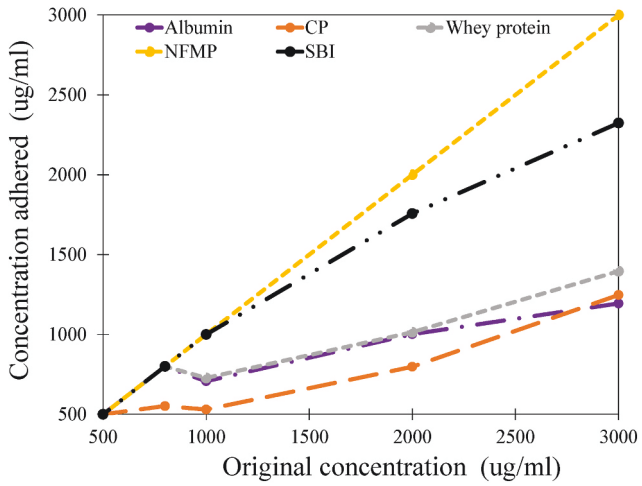

Fig. 2. Adsorption isotherm of proteins on wollastonite particles.

bearing groups - and hydrophobic forces [26], the proteins are equipped with multiple pathways to interact with and adsorb onto the wollastonite particles surface. This is particularly relevant in the case of NFMP, and it can be seen that unlike the other proteins, NFMP showed a maximum adsorption within the concentrations studied despite exhibiting relatively low negative charge. The self-aggregation of NFMP and formation of insoluble protein aggregates can occur in the pore solution of wollastonite suspension; when this occurs, the insoluble protein aggregates leave the solution, and this can potentially erroneously contribute to the high adsorption values measured from the experiments. It has been reported that casein, which comprises 80% of NFMP, has the tendency to chelate Ca^{2+} and form insoluble aggregates in Ca^{2+} rich and high pH environment [31,41].

3.1.3. Flow test

The results of the flow test performed on the fresh wollastonite paste modified with 0.25%, 0.5%, and 1% concentration of protein and a control without proteins are shown in Fig. 3. Generally, it can be observed that the addition of the proteins increased the flowability of the wollastonite paste compared to the control except in the case of NFMP. Through the addition of proteins, the workability of cementitious materials can be improved by increasing the electrostatic repulsive forces between the particles of the cementitious materials [42]. The dispersing performance of the proteins may be associated with the adsorption of the proteins onto the surface of wollastonite particles [43,44]. In the wollastonite environment, the proteins assume a negative charge and are able to adsorb on the silicate phases through the bridging effect of Ca^{2+} [45]. The adsorption of the proteins onto wollastonite particles increases the surface charge as shown from the zeta potential analysis depicted in Fig. 1, which brings about increased electrostatic repulsion and consequently the flowability of the wollastonite pastes is increased [46]. This mechanism is similar to the rheological properties exhibited by fresh cement paste in contact with colloidal polymer particles observed in the previous study [43].

As the adsorption plateau is reached, increasing amount of free proteins in the interstitial fluid phases increases the flow due to the ball-bearing effect [43] and creation of air bubbles. Since, the proteins contain hydrophobic groups in the molecular structure, they can act as a surfactant and promote formation of air-bubbles in the interstitial fluid in the paste [47]. Thus, the increase in protein concentration is expected to increase the amount of free proteins in the interstitial fluid leading to increased flowability of the paste. This mechanism explains the observed increased flow with an increase in concentration of the proteins in the wollastonite paste.

The flow of NFMP modified wollastonite paste seems to follow the opposite trend although the flow increases as the protein concentration increases. Since the molecular structure of the proteins consist of a wide array of amino acids with varied functional groups that can interact with wollastonite particles surfaces, it is possible that different segments of NFMP adsorb onto different wollastonite particles providing a bridge between the wollastonite particles promoting flocculation of wollastonite particles in the paste. Thus, the mobility of wollastonite particles in the paste is hampered and the flow is reduced. The findings by Brzyski et al. [42] showed that the addition of casein, the primary constituent of NFMP, to cementitious paste leads to the formation of casein glue which makes the pastes sticky and subsequently reduces flow. Similarly, the restriction to flow in cementitious materials due to the formation of gels by polyacrylamide has been reported in previous studies [48]. The flow in the case of the pastes with NFMP appeared to increase with increased concentration of the proteins as the amount of free proteins that are not adsorbed onto wollastonite particles increase and that enhance the flow of the paste due to the ball bearing effect [49].

3.1.4. Surface tension

The effect of the proteins on the surface tension of extracted wollastonite pore solution is shown in Fig. 4. It can be observed that the surface tension of the protein modified extracted pore solution is lower than that of the control pore solution. The pH of the wollastonite paste was measured to be around 8.8. Since this pH is above the isoelectric points of the proteins, the proteins may undergo molecular and conformational changes and begin to unfold to expose the hydrophobic

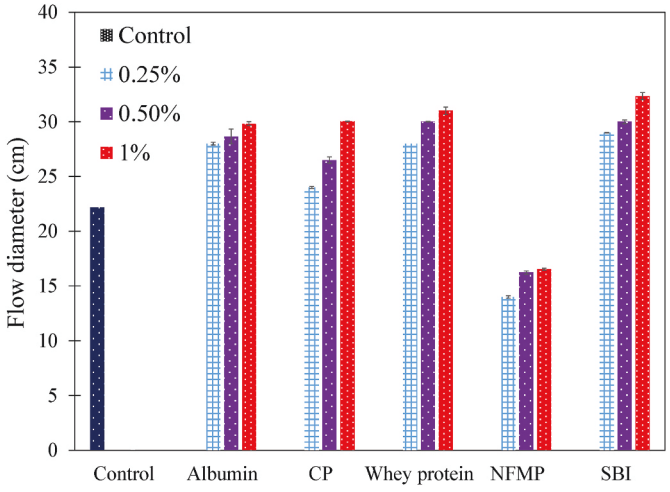

Fig. 3. The influence of admixed proteins on the flowability of wollastonite paste.

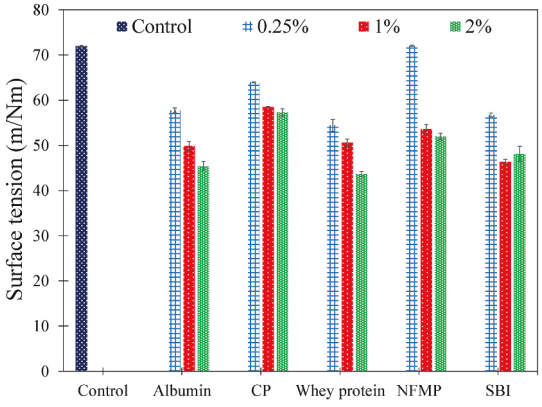

Fig. 4. The influence of admixed proteins on the surface tension of wollastonite solution.

groups [33,37,50,51] which contribute to a lower surface tension. The exposed hydrophobic groups adsorb onto the air-water interface and reduce the surface tension of the pore interstitial fluid in wollastonite paste [52]. It is seen that generally the surface tension seems to decrease with increasing concentration of the proteins; since, a portion of the proteins is adsorbed onto the wollastonite particles surfaces and only the free proteins in the interstitial fluid affect surface tension, the increase in concentration increases the amount of free proteins in the interstitial fluid and lowers surface tension.

It is seen that the surface tension of the extracted pore solution of albumin, whey protein and SBI modified wollastonite paste was slightly lower than that of CP and NFMP modified wollastonite paste at their respective concentrations. The higher surface tension of the extracted pore solution of the paste with CP could be due to the lower concentration of hydrophobic segment in the molecular structure of CP. The higher surface tension of CP compared to other proteins in the pore solution of Portland cement has also been documented in a previous study [37]. The insignificant change in surface tension in the case of NFMP at low concentration (0.25%) could be a result of insignificant amount of free proteins in the pore solution as a result of protein adsorption onto wollastonite particles and insoluble protein aggregate formation [31]. This rationale is supported by the fact that at higher concentrations the surface tension depicted a marked reduction indicating the presence of free proteins in the pore solution. According to the Kelvin-Laplace equation, the capillary forces in the pore structure is directly proportional to the surface tension of the pore solution [6]. Thus, the reduced surface tension of the pore solution in the case of the pastes with the proteins could have important implications in the potential creation of cracks due to shrinkage as the reaction products are precipitated and fine capillary pores start to form in the microstructure.

3.1.5. Water contact angle

Water contact angle measurements were taken on the carbonated wollastonite paste to investigate the hydrophobicity of the pastes with or without proteins. As shown in Fig. 5 it is demonstrated that the protein modified carbonated wollastonite paste generally showed higher water contact angle than that of the control, which is in line with the effect of protein on the surface tension of the pore solution as depicted in Fig. 4. Literature on water contact angle of carbonated wollastonite paste is difficult to find. Proteins are hydrophobic biomolecules which have the potential to induce water repelling effect on the pore surface in the microstructure of materials [37,53]. For instance, the modification of the pore and capillary structure through the formation of hydrophobic surfaces have been reported by Chandra and Aavik [39,54] and Baffoe and Ghahremaninezhad [37] though the above mentioned studies were conducted on Portland cement mixtures. In the pore structure of the carbonated wollastonite paste, it is plausible that the hydrophilic components of the proteins attach to the pore surface while the hydrophobic components extend out at the air-solid interfaces, thus hydrophobizing the pore surface in the microstructure.

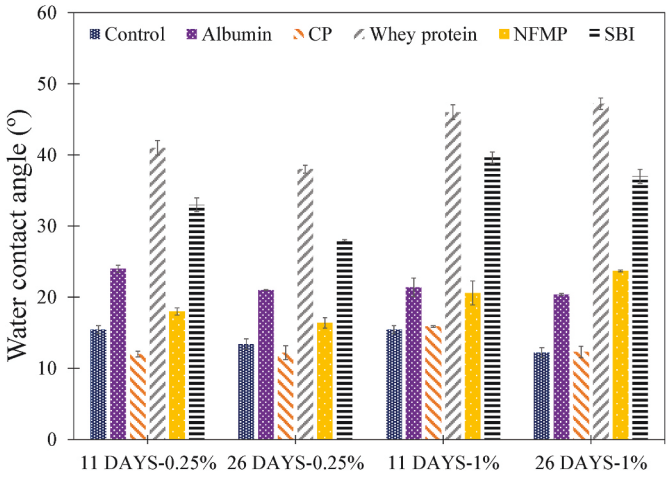

Fig. 5. The influence of admixed proteins on the wetting performance of carbonated wollastonite pastes.

Among the protein modified carbonated wollastonite pastes, it can be observed that the water contact angles of CP and NFMP carbonated pastes were lower than that of the albumin, whey protein and SBI modified carbonated wollastonite pastes. This possibly can be attributed to higher surface tension of the pore solution exhibited by CP and NFMP as shown in Fig. 4. Based on prior studies, surface tension of the pore solution has been shown to be an indirect measure of surface hydrophobicity, that is, a lower surface tension indicates a higher surface hydrophobicity [37,55,56]. Evidently, the relatively higher contact angle of whey protein and SBI modified carbonated wollastonite paste directly correlates with the low surface tension of these proteins. CP demonstrated the lowest adsorption as shown in Fig. 2; thus, this can also contribute to small contact angle and low hydrophobization effect of CP compared to other proteins investigated here. A study on the low water contact angle and hydrophobization of CP on other cementitious substrates was reported by Baffoe and Ghahremaninezhad [37].

3.2. Microstructural properties

3.2.1. FTIR

The FTIR spectra of the wollastonite carbonate pastes with or without protein was collected to investigate the chemical characteristic of the carbonated wollastonite pastes and to identify the polymorphs of the $CaCO_3$ formed. The pastes showed similar FTIR peaks at both concentrations of 0.25% and 1% so only the results of the 1% protein carbonated pastes are shown and discussed here except the result of the albumin carbonated pastes where the result of both concentrations are shown. It must be emphasized that the peaks below 700 cm^{-1} are characteristic peaks of the calcium and silica-containing phases of the wollastonite pastes and other uncarbonated phases such as quartz, anorthite which are added impurities during production [7,12].

From Fig. 6, the peaks at 712 cm^{-1} and 874 cm^{-1} correspond to the formation of calcite [22]. The peaks were smaller at the initial stages of the carbonation process; however, it is noticed that the intensity of these peaks became stronger as the carbonation proceeded. This indicates that the quantity of calcite increased as the amorphous calcium carbonate (ACC) in the wollastonite carbonated pastes transformed into calcite. The broad band between 1060 cm^{-1} -1100 cm^{-1} and 896 cm^{-1} is assigned to the asymmetric stretching vibration of (ν_3) of the Si–O bond in the mineral [57]. The position of the Si–O bond was observed to shift to high wavenumbers or disappear with increasing carbonation period. This observation is attributed to the increased polymerization of the silicate gel [16,58]. As shown in Fig. 6a, the control paste showed a broad peak around 1434 cm^{-1} at 6–18 h of carbonation but shifted to 1420 cm^{-1} with a sharper peak after 72 h of carbonation period. This indicates the conversion of ACC to stable calcite in the control paste due to extended period of carbonation [22,59]. The peak located at 1797 cm^{-1} is an indicative of the presence of $CaCO_3$ [37,60] and it was shown to increase with carbonation time.

Fig. 6b and c shows the FTIR analysis of the albumin carbonated paste. The in-plane vibration (ν_2) at 856 cm^{-1} and the ν_3 vibration of CO_3^{-2} ions at 1450 cm^{-1} along with the weak peak at 700 cm^{-1} indicate the presence of aragonite in the paste [61]. The gradual increase in intensity of peaks at 856 cm^{-1} and 1450 cm^{-1} in Fig. 6b indicates the transformation of some ACC into aragonite phases [61]. The presence of a peak at 712 cm^{-1} indicates the $CaCO_3$ polymorph is a mixture of calcite and aragonite, and this occurred in both Fig. 6b and c. It can therefore be postulated that the albumin carbonated paste will have some aragonite phases in the microstructure but generally, the microstructure of this paste will likely have calcite as the predominant polymorph.

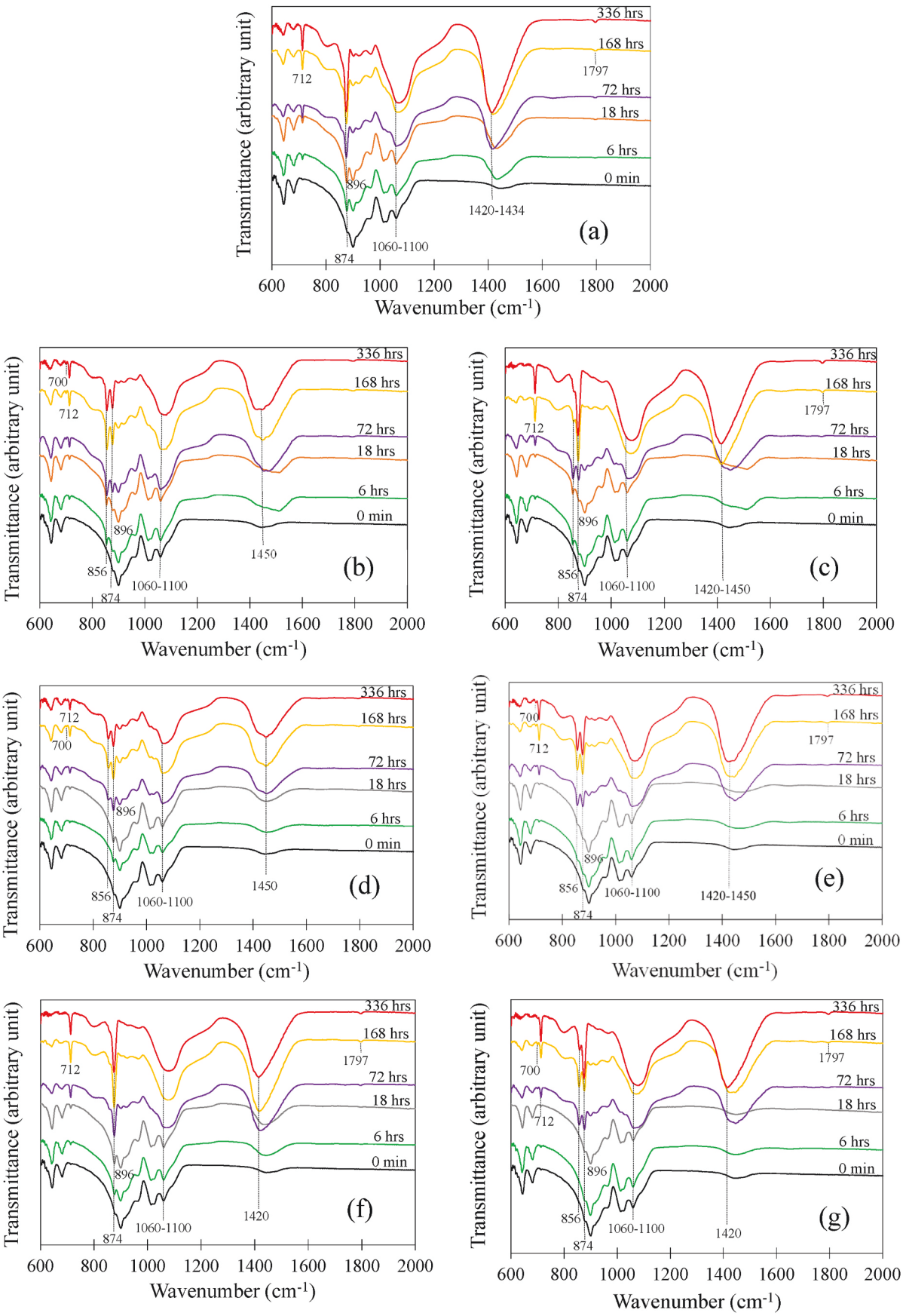

Fig. 6. The FTIR spectra of carbonated paste (a) without any protein, (b and c) with 0.25% and 1% albumin, respectively (d) with 1% CP, (e) with 1% whey protein, (f) with 1% NFMP, and (g) with 1% SBI, respectively with carbonation duration.

The FTIR characteristic peaks of CP carbonated paste shown in Fig. 6d were similar to the albumin carbonated paste. After 72 h of carbonation, the ν_3 vibration of the CP carbonated paste showed a peak at 1450 cm^{-1} along with a weak peak at 700 cm^{-1}. This could be an indication of small amount of aragonite in the microstructure [61]. Again, it is noticed that the peak at 712 cm^{-1} was not intense as it occurred in the control paste and the albumin carbonated paste. This could be a result of lower carbonation of CP carbonated paste at this period of carbonation time.

In Fig. 6e, the FTIR characteristic of whey protein carbonated paste presented a sharp peak at 712 cm^{-1} after 336 h of carbonation period, indicating the presence of calcite polymorphs [22]. In Fig. 6e, a peak (856 cm^{-1}) associated to aragonite formation can be identified after 168 h of carbonation, possibly an indication of aragonite stabilization [61]. Typical of ACC and aragonite polymorphs, it is seen that the band between 1420 cm^{-1} to 1450 cm^{-1} appeared broader along with a weak peak at 700 cm^{-1} in the 1% whey protein carbonated paste [61].

The sharp ν_4 out-of-plane peak at 712 cm^{-1} as observed in the NFMP carbonated paste (Fig. 6f) indicated the presence of calcite in the microstructure [23]. The predominance of calcite as the primary polymorph in the NFMP carbonated paste is also demonstrated by the narrow stretching vibration of the ν_3 peak located at 1420 cm^{-1} [7]. No traces of aragonite polymorphs were identified in the NFMP carbonated paste.

The SBI carbonated paste (Fig. 6g) exhibited similar FTIR peaks to the NFMP carbonated paste. At the initial stages of carbonation ACC

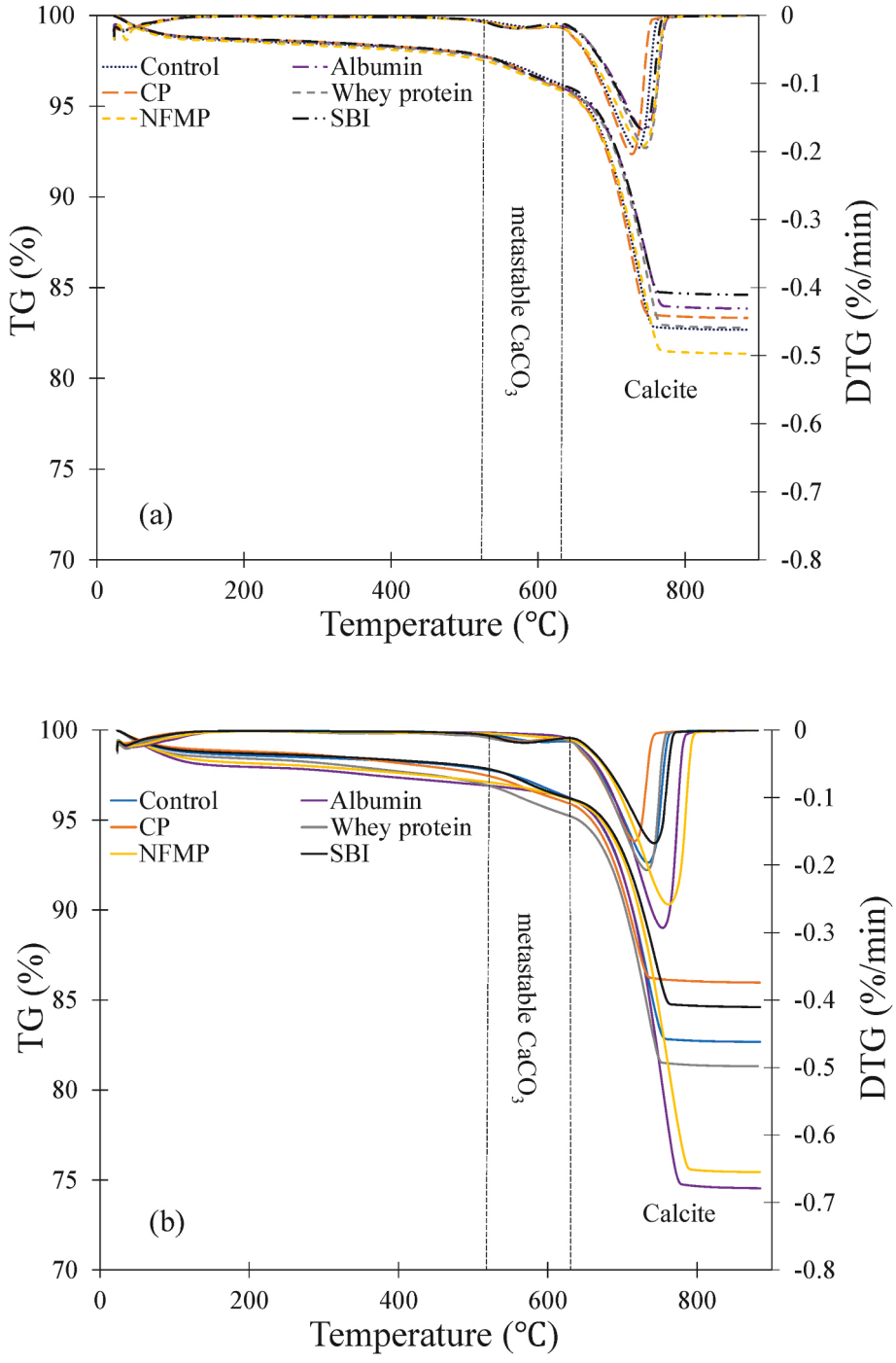

Fig. 7. TGA and DTG curves for (a) 0.25% and (b) 1% wollastonite paste carbonated for 168 h.

occurred as the predominant polymorph in the microstructure. However, after 168 and 336 h of carbonation, the ACC gradually transformed into stable calcite and aragonite phases (see Fig. 6g) as can be seen by the sharp and intensified peaks at 712 cm^{-1}, 856 cm^{-1}, 874 cm^{-1} and 1420 cm^{-1} respectively [7,61]. The aragonite peak appears to be weakened after 336 h of carbonation reaction. Like the control paste, it is instructive to note that the predominant polymorph of the SBI carbonated paste is calcite.

The predominance of calcite as the main $CaCO_3$ polymorph is not surprising as the formation of specific polymorphs is dependent on various factors such as the type of calcium silicate phase and environmental conditions under which the test was performed [16]. During the Ostwald's process, ACC is first to form which then transforms to vaterite or aragonite (metastable) and finally more stable calcite [62]. In the presence of biomolecules such as amino acids or proteins, these biomolecules can adsorb onto the forming vaterite or aragonite phases and prevent their transformation to more stable calcite [22]. This process does not always occur as the carbonation path is sometimes affected by other factors such CO_2, pH, etc. These factors may hasten the crystallization transformation directly from ACC to more stable calcite.

Due to the low concentration of proteins used, peaks corresponding to the protein molecular structure were not identified.

3.2.2. TGA

Fig. 7a and b shows the TGA and DTG of the carbonated wollastonite pastes after 168 h of carbonation period. The derivative and mass loss from the matrixes can be categorized into two stages. These stages of carbonation were noticed to have occurred between 530 °C to 620 °C and 620 °C to 900 °C, respectively [63] and are attributed to the decomposition of $CaCO_3$. Loss of chemically bound water was observed to have not occurred in the pastes. This observation is consistent with the findings made by Ref. [64]. As shown in Fig. 7, the mass loss which occurred between 530 °C to 620 °C is attributed to the decomposition of poorly crystalline or metastable polymorphs which include ACC, vaterite and aragonite [65,66]. The mass loss which occurred in the region of 620 °C to 900 °C is attributed to the decomposition of calcite [63] which is described as a well crystalline form of $CaCO_3$ [63]. It is apparent from the TG/DTG curve that some protein carbonated pastes exhibited relatively higher decomposition of total $CaCO_3$.

The $CaCO_3$ content of the carbonated wollastonite pastes comprising metastable phase and crystalline calcite with or without protein is shown in Fig. 8. $CaCO_3$ content increased with increasing carbonation time as observed in Fig. 8. It can be seen that at 6–72 h, the $CaCO_3$ content of most of the protein carbonated pastes was lower than that of the control. The adsorption of the proteins onto the wollastonite particles can impede the exchange of Ca^{2+} at wollastonite particle and solution interface. The early carbonation reaction of wollastonite paste is affected by the dissolution of Ca^{2+} and silicate ions, therefore the reduced ionic exchange due to protein adsorption is likely to delay the carbonation of $CaSiO_3$ and retard the formation of $CaCO_3$ during the first 72 h.

However, at 168 h and 336 h, the $CaCO_3$ content of the protein carbonated pastes, particularly in the pastes with 1% protein, is higher than that of the control. As discussed previously in Figs. 4 and 5, the proteins due to the presence of hydrophobic functional groups in their molecular structure can induce surface hydrophobization in the pore structure of the pastes. This is evident from the increase in surface contact angle of the pastes with the proteins as shown in Fig. 5. The increase in hydrophobic characteristics of the pore structure result in delayed water loss due to evaporation [5] and as a result the free water needed for the carbonation reaction to continue is expected to remain available in the paste with the proteins while in the control paste the free water is expected to dry out. This mechanism is expected to contribute to higher $CaCO_3$ content in the paste with protein compared to the control paste. The effect of evaporation of free water and drying out of carbonated wollastonite pastes on reducing carbonation reaction was also evidenced in a prior study [16].

Proteins can adsorb onto solid surfaces [26] including carbonated wollastonite particles, reduce the activation energy of nucleation and facilitate the growth of $CaCO_3$ by providing sites for carbonation products to grow around it [21,46]. It has been reported that the acidic and basic dominated amino acids in proteins promote the nucleation of $CaCO_3$ [66,67]. Therefore, after 168 h, the nucleation effect, coupled with the better dispersion of the wollastonite particles, could enhance the carbonation reaction in the pastes with the proteins. It is noted that generally, 1% protein carbonated pastes showed higher $CaCO_3$ content compared to the 0.25% protein carbonated pastes. Carbonation is influenced by moisture content as the uptake of CO_2 has been shown to be influenced by the amount of free water present in the pastes. Though the RH was same for all pastes, the rate of evaporation and drying out is expected to be slower in the paste with 1% proteins compared to the pastes with 0.25% proteins. This can explain the increased $CaCO_3$ in the pastes with 1% proteins, particularly at later ages of carbonation as seen in Fig. 8.

Fig. 9 is the TGA results of the pastes taken from the core of the 25 mm × 25 mm cube pastes. With the exception of one or two pastes, it is seen that the $CaCO_3$ content of the 26-day carbonated pastes was similar to the 11-day carbonated pastes. This is because, once a certain degree of carbonation reaction has taken place starting from the exterior of the pastes, diffusion of CO_2 into interior of the wollastonite pastes is

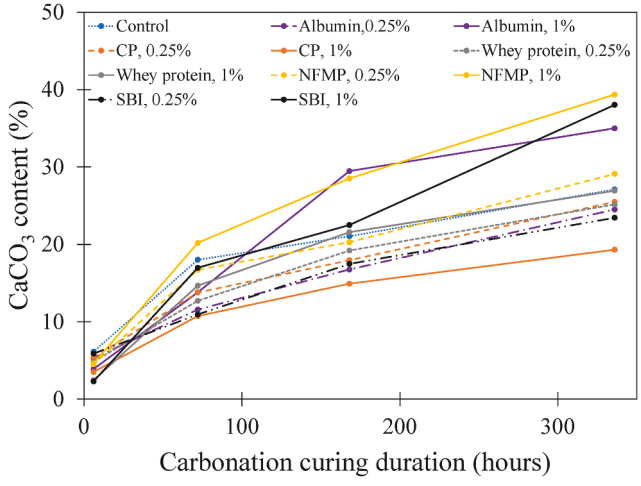

Fig. 8. Total $CaCO_3$ content of carbonated wollastonite pastes with carbonation duration.

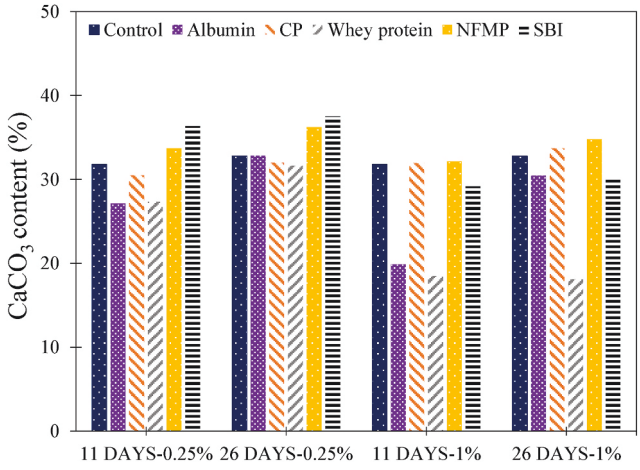

Fig. 9. Total $CaCO_3$ content in bulk 25 mm × 25 mm × 25 mm carbonated wollastonite pastes at different carbonation durations.

hampered by reduced porosity of the microstructure near the exterior of the paste [57].

The 1% whey protein carbonated pastes showed significantly lower $CaCO_3$ content at both 11 days and 26 days, compared to pastes with other proteins. To explore this further, a small piece with an approximately 2 mm thickness from the exterior surface of this paste was ground into powder and tested using TGA. The TGA results showed that the $CaCO_3$ content of the exterior was approximately 30.3%. Thus, this confirms that the growth of $CaCO_3$ is more pronounced on the exterior especially for bulk pastes in this study. This is in support of the observations made by Min and Jun [68], Thiery et al. [69] and Silva et al. [18].

It is noted from Fig. 9 that the pastes with lower protein content (0.25%) generally demonstrated a lower $CaCO_3$ content compared to the pastes with higher proteins (1%). One explanation for this could be the higher carbonation reaction on the exterior of the paste with 1% proteins compared to the pastes with 0.25% protein resulting in reducing the diffusion rate of CO_2 to the interior of the pastes. This is line with the $CaCO_3$ content results at late ages discussed in Fig. 8. In addition, increased hydrophobicity of the pore surface due to higher protein content could have also affected the CO_2 diffusion into the interior of the paste [37].

3.2.3. XRD

The XRD pattern of carbonated wollastonite pastes with 0.25% or 1% protein concentration and exposed to 168 h of carbonation period are shown in Fig. 10a and b, respectively. Peaks 1, 2, 3 and 4 represent wollastonite, calcite, aragonite and vaterite respectively. Peaks related to unreacted wollastonite and $CaCO_3$ were uniquely identified. Unreacted wollastonite particles showed peaks at 2 θ of 23.2°, 25.3°, and 26.9° along with some other peaks which appeared very weak [16]. The absence of silica gel in the XRD spectra is due to the amorphous nature of this phase [7]. The $CaCO_3$ basically showed three different polymorphs namely calcite, aragonite and vaterite which were distinctly present at 2 θ of 29.4°, 2 θ of 35° and 2 θ of 30.5° [7,16] respectively. The various phases revealed in the XRD spectra are in accordance with the FTIR results presented in Fig. 6 and supported by the literature [16]. The control paste showed traces of aragonite, but calcite was the main polymorph. The weak intensity of aragonite confirms the relatively low stage 2 mass loss identified in the TGA results and weak peaks seen in the FTIR results. At 0.25% of protein concentration albumin, whey protein, NFMP and SBI carbonated wollastonite pastes showed similar peaks to the control paste. These peaks demonstrated that calcite is the dominant polymorph.

The average peak intensity of calcite in the control and the 0.25% protein carbonated pastes were similar and this observation is consistent with the findings of the TGA results presented in Fig. 8. At 1%, some of the protein modified carbonated pastes presented a peak intensity that was noticeably higher than that of the control after 168 h of carbonation time. For instance, the albumin and NFMP carbonated pastes showed much higher calcite peaks compared to the control. This supports the above discussion-findings on the TGA results presented in Fig. 8 where it was shown that overall, the albumin and NFMP carbonated pastes showed higher $CaCO_3$ than that of the control after 168 h of carbonation time.

In addition, it can be seen that the albumin and NFMP carbonated paste showed an additional peak at 2 θ of 30.5° which corresponds to vaterite phase. Due to the low intensity of the peak assigned to vaterite, it is not surprising that vaterite which usually occurs at a frequency of 745 cm^{-1} did not show up in the FTIR results shown in Fig. 6c and f. The

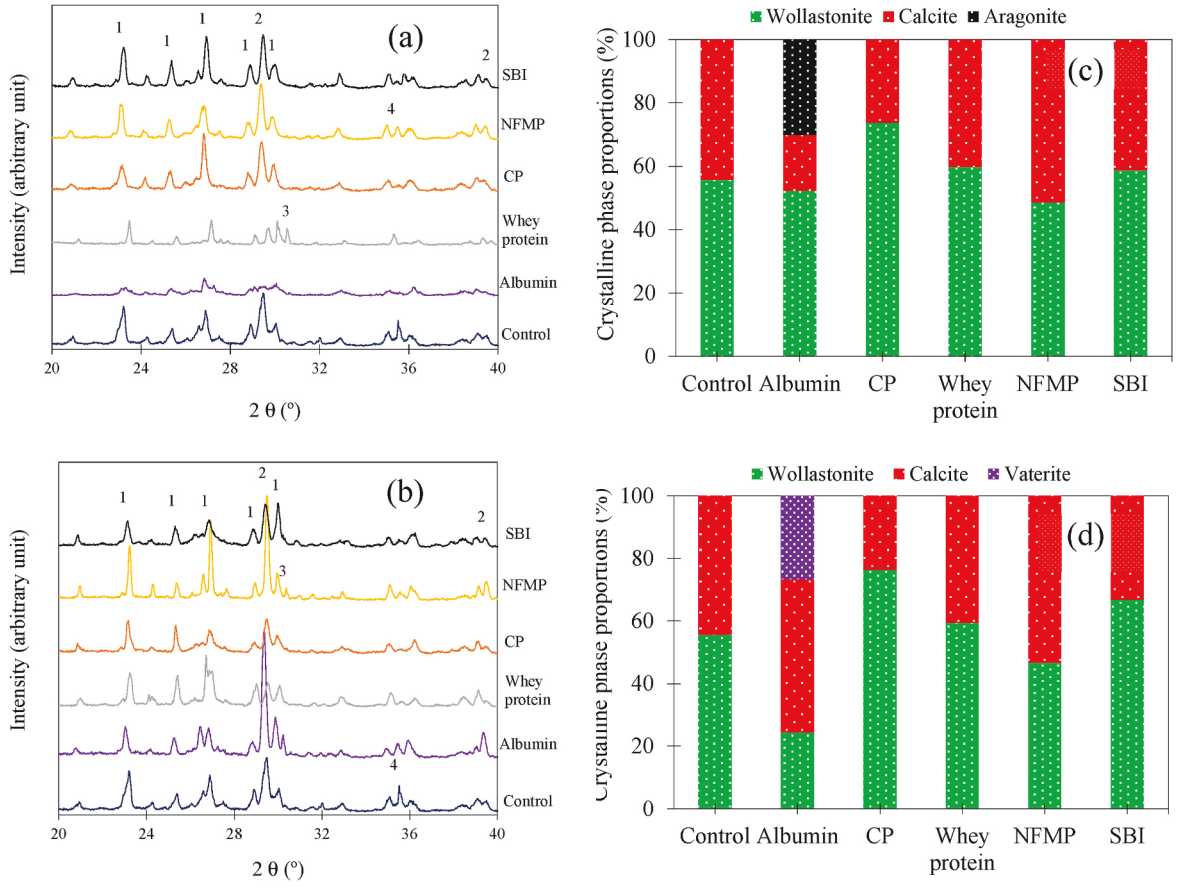

Fig. 10. X-ray diffraction pattern of (a) 0.25% and (b) 1% wollastonite paste carbonated for 168 h and their respective quantitative crystalline phase proportions as (c) and (d), respectively. Peaks 1, 2, 3 and 4 represent wollastonite, calcite, aragonite and vaterite, respectively.

relative proportion of the crystalline phases in the carbonated pastes was semi-quantified by performing Rietveld refinement and reported in Fig. 10c and d, for the carbonated wollastonite pastes with 0.25% and 1% proteins, respectively. The presence of ACC was not identified in the phase analysis due to their lack of crystallinity and relatively small quantity. CP carbonated paste showed the highest quantity of wollastonite particles indicating lower degree of carbonation reaction. The higher wollastonite particles but lower calcite content in the case of CP carbonated paste is consistent with the FTIR and TGA results shown in Figs. 6 and 8, respectively. The amount of calcite was highest in albumin and NFMP carbonated pastes. This is consistent with the TGA and XRD patterns in Figs. 8 and 10b, respectively and further confirms that the addition of some proteins enhanced the carbonation reaction, particularly at late ages under the carbonation conditions used in this study. It can be seen that the albumin carbonated paste showed the formation of some amount of aragonite and smaller content of vaterite in addition to calcite. The presence of aragonite was also noted in the FTIR results discussed in Fig. 6.

3.2.4. SEM

Fig. 11 shows the SEM images of the carbonated wollastonite pastes. The SEM images were taken of wollastonite carbonated thin pastes on the glass slides (a, c, e, g, i, k) for 168 h and ground into powder. In addition, the SEM images of the fractured surfaces of the 25 mm × 25 mm bulk pastes with or without 1% protein concentration (b, d, f, h, j, l) and carbonated for 26 days were investigated. Owing to the differences in carbonation time, it is expected that the pastes from the fractured surfaces will generally be more carbonated compared to the pastes carbonated on the glass slide. This is consistent with the effect of time on the extent of carbonation shown in Figs. 8 and 9.

In the microstructure of the carbonated wollastonite pastes, three different phases can be identified, namely, partially reacted/unreacted wollastonite particles, calcium modified silica gel, amorphous calcium carbonate and crystalline $CaCO_3$ [70]. The SEM images of the microstructure of the control (thin paste and fracture surface) is shown in Fig. 11a and b. Consistent with the results presented in Fig. 6a, the presence of spherical shaped particles aggregated together can be seen in Fig. 11a with a higher magnification inserted. These spherical shaped particles could be ACC [71] and they were seen to be clustered around cubic or rhombohedral crystals of calcite or the partially reacted wollastonite particle. The presence of partially reacted wollastonite is also indicated in Fig. 10b and d. In Fig. 11b, the control paste demonstrated the presence of numerous cubic and rhombohedral calcites. The stark difference in calcite content between Fig. 11a and b is in support of the higher $CaCO_3$ content as discussed in the TGA results shown in Figs. 9 and 8.

Fig. 11c and d showed the microstructure of albumin carbonated pastes. The microstructure of Fig. 11c showed some ACC clustered

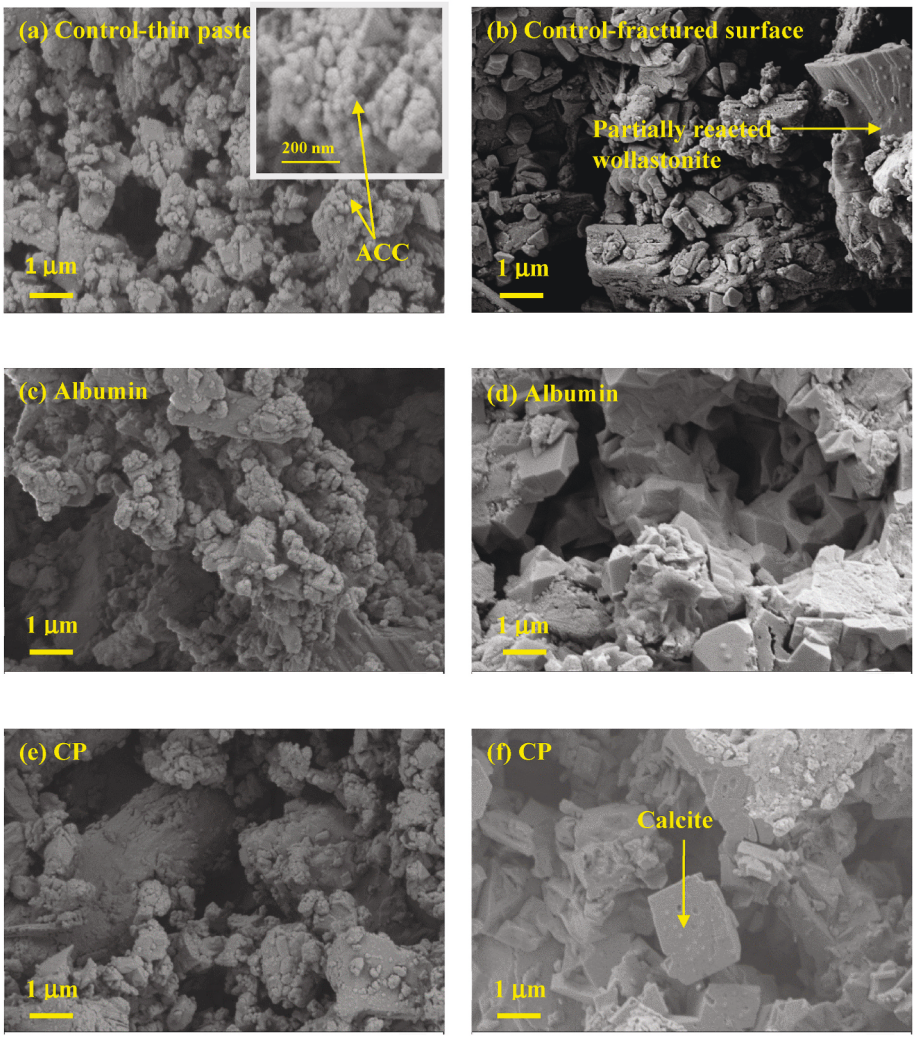

Fig. 11. SEM of carbonated pastes showing phases of partially reacted wollastonite, ACC and crystalline $CaCO_3$ with or without 1% protein concentration. (a, c, e, g, i, k) are 168-h thin paste carbonated samples while (b, d, f, h, j, l) are fractured surfaces of the bulk 25 mm × 25 mm × 25 mm 26-days carbonated cubes.

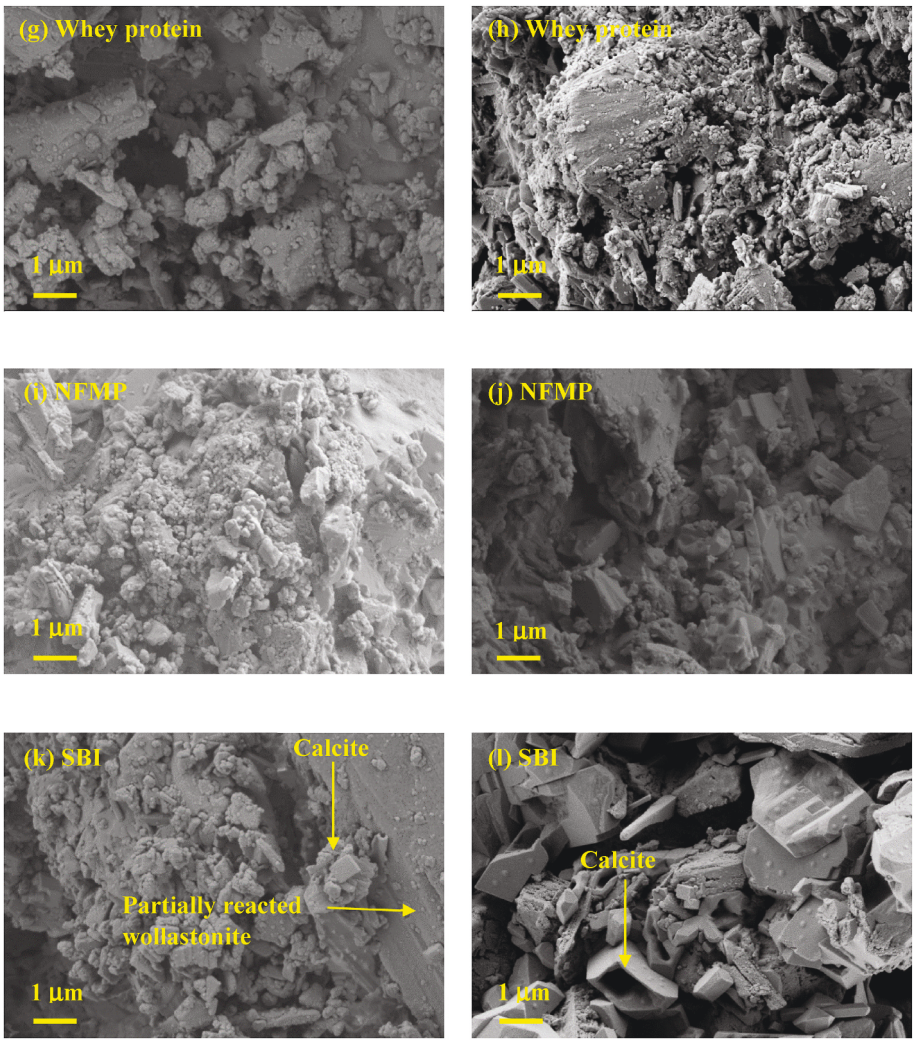

Fig. 11. (*continued*).

around calcite and some partially reacted wollastonite while in Fig. 11d, one can identify phases that resemble calcites. The presence of vaterite and aragonite was difficult to identify in the SEM of the wollastonite pastes with albumin. Vaterite polymorph was seen to be present in Fig. 10d but absent in Figs. 6c and 11c, which could be due to a small amount of this phase present in the microstructure.

Fig. 11e and f showed the microstructure of CP carbonated pastes. CP carbonated pastes in Fig. 11e showed the presence of calcite and some ACC clustered around partially reacted wollastonite particles. This was, however, not the case in Fig. 11f. In Fig. 11f, it was revealed that the predominant phase was calcite with little or no ACC present. The calcites assumed cubic shapes and were generally bigger in size compared to the control. The presence of calcite as the predominant polymorph is consistent with the results discussed in Figs. 6d and 10d.

The microstructure of whey protein carbonated wollastonite pastes in Fig. 11g and h was found to have some ACC deposited on partially reacted wollastonite, nonetheless, portions of the paste was shown to consist of calcite. The reduced $CaCO_3$ in Fig. 11h agrees with the findings in Fig. 9, related to the 1% whey protein modified pastes carbonated for 26 days. A comparison between Fig. 11i and j revealed that the microstructure of the NFMP carbonated paste was a mixture of ACC, partially reacted wollastonite particles and calcites.

The SEM of the SBI carbonated paste in Fig. 11k showed the presence of calcites and partially reacted wollastonite. The presence of other metastable phases (vaterite and aragonite) was difficult to identity possibly due to the low amount of these phases in the microstructure. This observation is consistent with the FTIR and XRD results shown in Figs. 6g and 10d. Fig. 11l also showed a predominant display of rhombohedral crystals of calcites. The sizes of these calcites were bigger than that of the control paste in Fig. 10b which could be due to the effect the delayed moisture loss had on the morphology of the calcites in Fig. 11l [64].

The presence of calcite as the predominant polymorph in all the carbonated pastes corroborates the findings of other studies [17] that calcite is the primary polymorph of carbonated wollastonite pastes. It is noted that some proteins affected the morphology of the calcites by increasing the sizes of calcites formed inside the microstructure.

3.3. Macroscale properties

3.3.1. X-ray micro-CT and drying shrinkage analysis

Micro-CT examination was performed to evaluate the internal microstructural characteristics of the control and the protein modified carbonated wollastonite pastes and also the drying shrinkage of the paste. Fig. 12 shows the drying shrinkage of the carbonated wollastonite paste with and without proteins. It is seen that the control sample exhibited higher shrinkage compared to the samples modified with proteins. In addition, the samples modified with whey protein and SBI demonstrated the lowest shrinkage compared to the samples modified with CP and NFMP. The shrinkage results seem to have a similar trend to

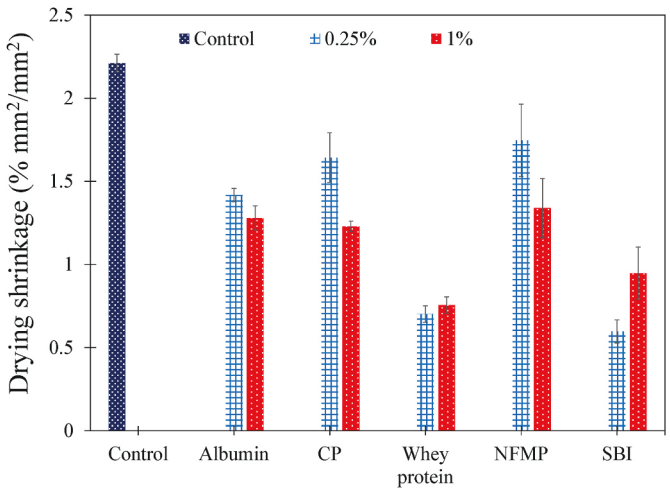

Fig. 12. Drying shrinkage of carbonated wollastonite paste with and without proteins.

the surface tension and water contact angle measurements shown in Figs. 4 and 5.

The 2 D reconstruction images of different pastes are shown in Fig. 13. The control paste presented in Fig. 13a shows cracks and air voids in the microstructure. The formation of cracks in the control paste can be attributed to drying shrinkage [72–74]. Prior studies did not investigate the development of cracks in carbonated wollastonite paste, if any [7,14,16].

It can be observed that the carbonated wollastonite pastes with 1% concentration of whey protein and SBI, did not show cracks in their microstructure as evident from Fig. 13d and f. On the other hand, the pastes with albumin, CP, and NFMP showed cracks. The volume fraction of cracks in the pastes are quantified and presented in Table 2. The volume fraction of crack in the control paste and the pastes with albumin, CP and NFMP was in the range of 2–4.5%. A comparison of the crack formation, drying shrinkage and water contact angle results of the pastes can shed light on the mechanisms responsible for cracking in some of the pastes. It appears that the crack formation is relatively correlated with the water contact angle, which is an indication of pore surface hydrophobicity, and pore solution surface tension in the pastes. It is seen that the pastes with SBI and whey protein exhibited higher contact angle values compared to the control and other proteins. These pastes (SBI and whey protein) also did not show cracks in the micro-CT results. The capillary forces are dependent on the contact angle and the surface tension of the pore solution as described by the Young-Laplace equation (1) below:

$$\sigma = -\frac{2\gamma \cos\theta}{r} \quad (1)$$

Where, σ is the capillary pressure, γ is the surface tension, θ is the water contact angle of the wall of the capillary pore, and r is the radius of the pore. It is seen that the capillary force is directly related to the pore solution surface tension and inversely related to contact angle. Thus, it is expected that the capillary forces are lower in the pastes with whey protein and SBI compared to the control and the pastes with other proteins. Since the control, CP and NFMP carbonated pastes are less hydrophobic, the water diffusion rate and consequently evaporation from these pastes is larger and that will result in the increased action of capillary stresses which increase drying shrinkage and promote crack formation. Thus, the above-mentioned observation provides strong evidence that drying shrinkage is an important factor in developing cracks in the pastes.

The microstructure of the carbonated wollastonite pastes modified with albumin, CP, whey protein, NFMP, and SBI at 0.25% concentration was also studied to explore the possibility of crack formation in these pastes and also to study the influence of this concentration on void formation. Overall, the paste modified with protein demonstrated a relatively similar cracking behavior at both 1% and 0.25% concentrations. As seen in Fig. 13i and k, whey protein and SBI modified pastes did not show cracking similar to what was observed at 1% concentration for these proteins. CP and NFMP modified samples showed cracking at both 1% and 0.25% concentrations as seen in Fig. 13c and e.

The presence of voids is observed in the microstructure of the pastes as seen in all pastes in Fig. 13. The total porosity of these voids was quantified and is presented in Table 2. The control paste showed some isolated large voids as seen in Fig. 13a. This can possibly be attributed to the mixing action or dissolved air in the wollastonite powder [75]. Generally, the protein carbonated wollastonite pastes showed an increased formation of voids compared to the control paste with the exception of SBI. The presence of voids in the protein carbonated wollastonite paste can be attributed to the surfactant functionality of the proteins, which reduces surface tension as at the air/water interface in the fresh paste contributing to the formation of stable air bubbles in the microstructure. As discussed, the unfolding of the proteins due to the relatively high pH of the wollastonite paste (pH = 8.8) exposes the protein hydrophobic groups. The adsorption of these hydrophobic groups at the air/water interface reduces the surface tension [47] and form a viscoelastic layer [76,77] possessing high surface shear viscosity that builds up air bubbles, stable enough to resist coalescence and collapse when formed in the paste [78]. In addition, the negatively charged functional groups of the proteins could interact with the Ca^{2+} released into pore solution and form insoluble sediment. These insoluble sediments and possibly other solid phases including wollastonite particles can be adsorbed on the bubble film to form a solid shell which has been reported to enhance the stability of air bubble [79].

Although the pastes with SBI and whey protein showed the highest reduction in pore surface tension as shown in Fig. 4, their void porosity was the lowest compared to the pastes with other proteins. This emphasizes the importance of other mechanisms discussed above that contribute to the stability of bubbles in the fresh paste [80]. In addition, if the surfactant has a higher hydrophobic character, it becomes too rigid or too insoluble and hence unable to induce foaming properties to the paste [81].

Of interest is a lower void porosity in the paste with 1% compared to 0.25% in the case of whey protein. A potential explanation for this could be due to increased flow and fluidity of the paste with whey protein with increasing concentration as discussed previously. With increased flow, conditions are favorable for air bubbles to escape from the wollastonite paste due to the force of buoyancy as stipulated by the Stoke's law [75].

The void size distribution and the average void size of the control and the 1% protein modified carbonated wollastonite pastes are shown in Fig. 14 and Table 2, respectively. Void sizes smaller than 0.050 mm were excluded in the analysis to avoid interferences from noise. The analysis in Fig. 14 excluded the presence of cracks in the microstructure. The void size distribution of the control and the carbonated paste with CP showed similar features, which was slightly different from that of the paste with other proteins, which also exhibited relatively similar characteristics. The average void size of the control paste was 0.29 mm while the albumin, CP, whey protein, NFMP and SBI carbonated pastes showed average void diameters of 0.22 mm, 0.28 mm, 0.11 mm, 0.19 mm, and 0.12 mm, respectively. Except for the case of CP, other proteins resulted in a smaller average void in the paste as seen Fig. 14 and Table 2. It is observed that CP seems to have had the least influence on the void size distribution and cracking in the pastes with the proteins. This observation is in agreement with the effect of CP on other properties discussed previously. CP had the lowest adsorption onto wollastonite particles, as shown in Fig. 2, which is an indication of its limited influence on the carbonation reaction and microstructure evolution of the pastes.

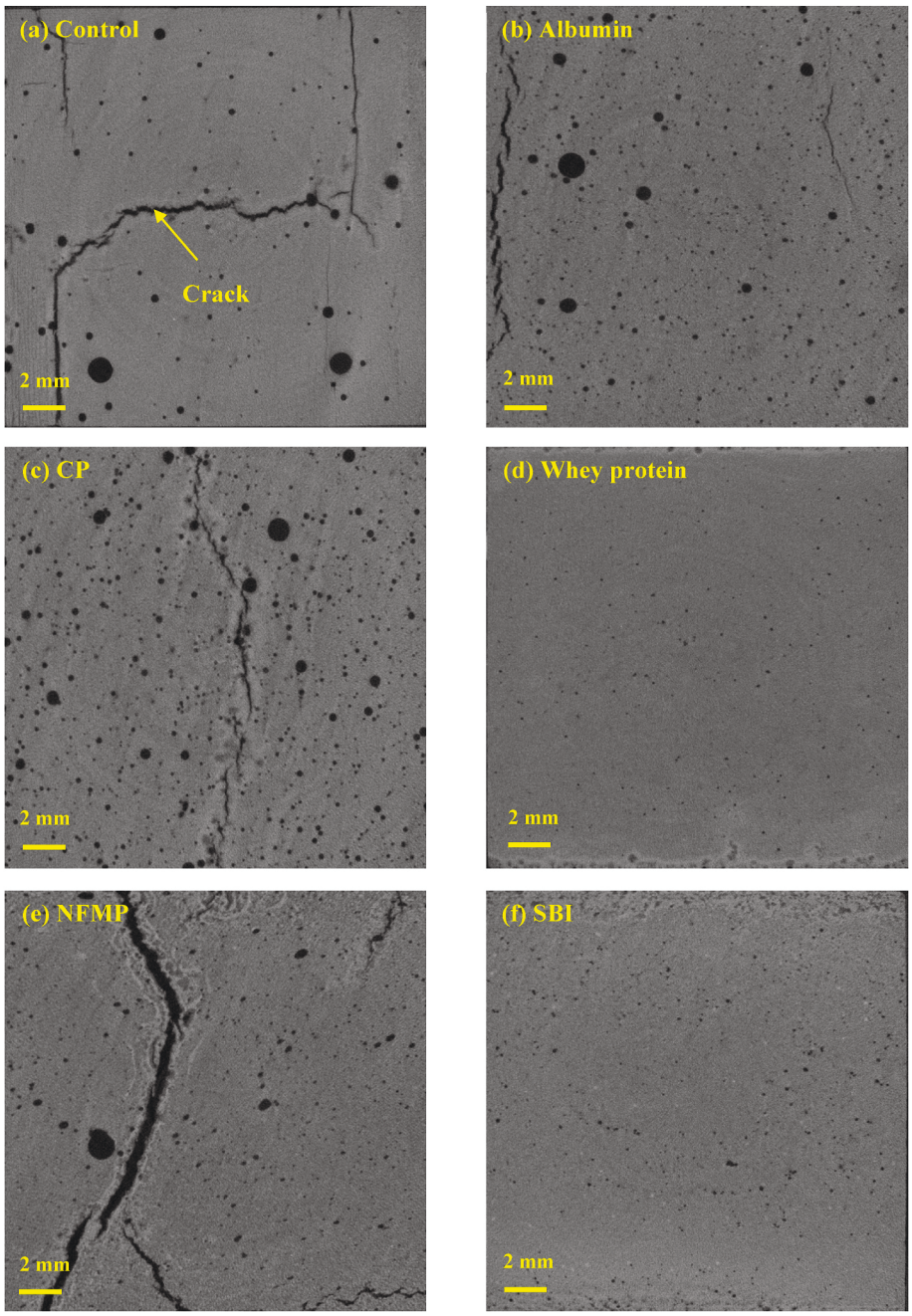

Fig. 13. 2 D representation of the reconstructed void structure for carbonated wollastonite pastes with (a) no protein (b–f) 1% protein and (g–k) 0.25% protein concentration.

3.3.2. Compressive strength

The effect of the proteins on the compressive strength of the carbonated wollastonite pastes is shown in Fig. 15. As shown in Fig. 15, the compressive strength of the 26-day carbonated wollastonite pastes was higher compared to the 11-day carbonated pastes. This is attributed to the continued carbonation process of the wollastonite paste, as more carbonation reaction products are accumulated in the pastes. It can be observed that generally the compressive strength of the carbonated wollastonite pastes modified with protein is higher compared to the control. The increase in compressive strength was more pronounced in the pastes modified with SBI, followed by whey protein, and albumin.

The cracks which occurred in the control paste could be a cause of the low strength as they act as stress concentration sites. But considering the similar or relatively bigger cracks in Fig. 13c and e and Tables 2 it is safe to argue that there are other multiple factors which contributed to the high strength of the protein modified pastes. The interfacial adhesive and Ca^{2+} crosslinking properties of the proteins could be one of the factors responsible for the improved compressive strength of these carbonated pastes. The negatively charged functional groups of the proteins can be crosslinked in the presence of Ca^{2+} leading to a dense molecular rigid network structure [26] which could promote the densification of the microstructure and enhance the compressive strength of these pastes [82].

As carbonation products are formed and replace water in the microstructure, the adhesive property of protein improves the interfacial strength between carbonation products in the microstructure resulting

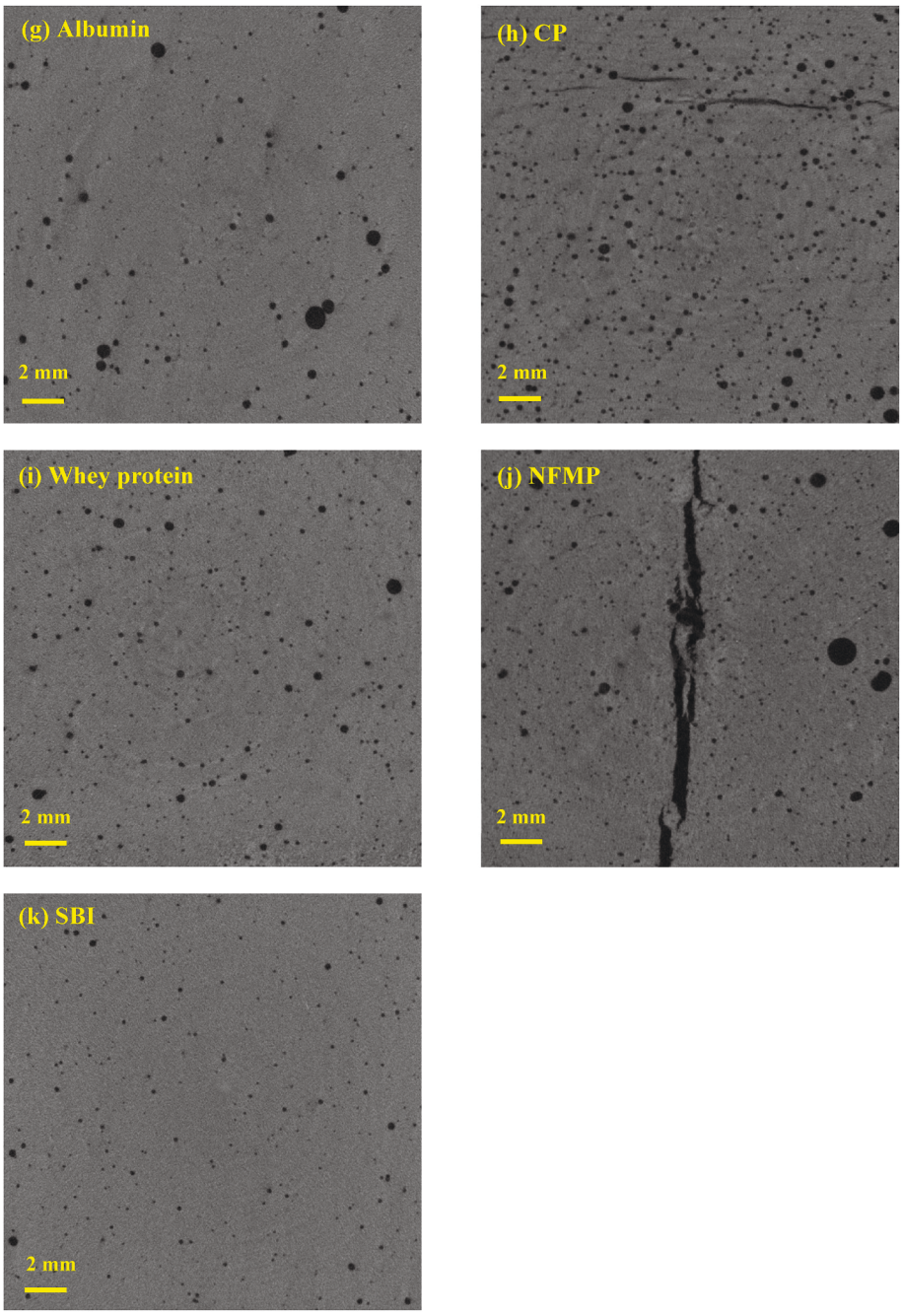

Fig. 13. (*continued*).

Table 2
Porosity and air void characteristics of the carbonated wollastonite pastes.

Sample	Air void (%)			Volume fraction of crack (%)			Total porosity (%)			Average void diameter (mm)	
	0%	0.25%	1%	0%	0.25%	1%	0%	0.25%	1%	0%	1%
Control	2.02			3.27			5.29			0.29	
Albumin		3.89	3.34			2.61		3.89	5.95		0.22
CP		5.76	4.50		0.89	3.13		6.65	7.63		0.28
Whey protein		2.18	0.55					2.18	0.55		0.11
NFMP		3.07	3.29		3.5	4.5		6.57	7.79		0.19
SBI		1.49	1.47					1.49	1.47		0.12

in improved compressive strength of the paste. In addition, as $CaCO_3$ is formed through the carbonation process, it is possible for some of the proteins to modify the morphology and micromechanical properties of the $CaCO_3$ and calcium modified silica gel formed, such as increasing the sizes of the calcites formed as presented in the SEM images. This leads to the formation of organic-inorganic composite microstructure, which has

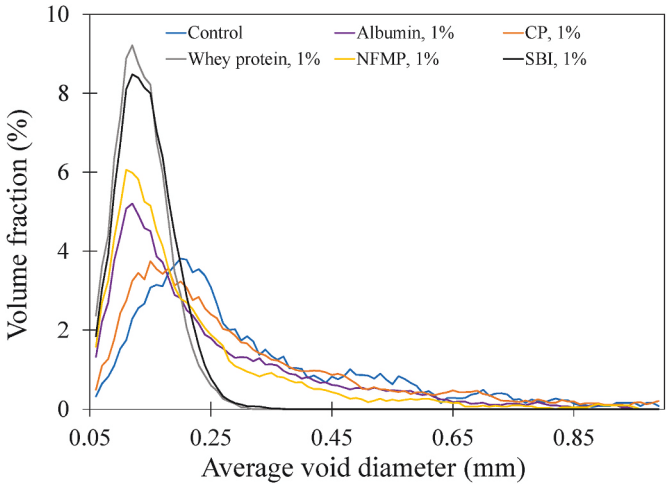

Fig. 14. Void size distribution of control and 1% protein modified carbonated wollastonite pastes after 26 days of carbonation period.

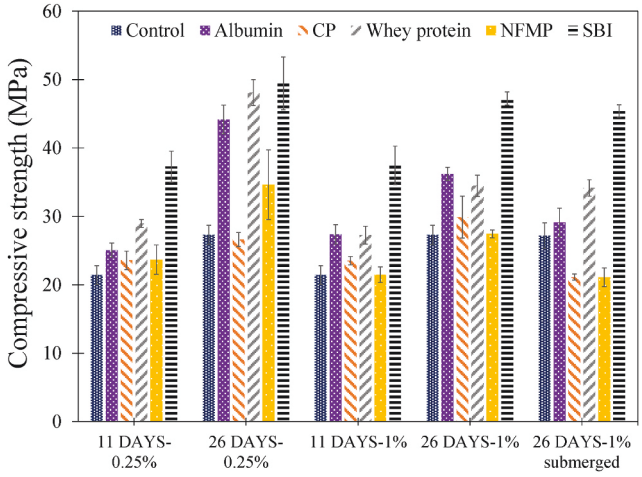

Fig. 15. The influence of proteins on the compressive strength of carbonated wollastonite pastes with different concentrations of proteins and durations of carbonation curing.

been reported to impart enhanced mechanical properties at the macro-scale [83]. Baffoe and Ghahremaninezhad [26] investigated the influence of biomolecules on enzyme-induced calcium carbonate (EICP) precipitation in ground hardened cement paste and observed an increased tensile strength of the bio-cemented paste modified with proteins. They attributed partly the increased tensile strength to the formation of organic-inorganic composite arising from the interaction between the proteins and EICP. In another study, Khan et al. [7] studied the influence of amino acids on the compressive and flexural strength of carbonated wollastonite paste and observed an increase in mechanical properties of the pastes modified with amino acids. In this study, the formation of organic-inorganic composite was suggested to be one of the reasons for the increased mechanical properties of the pastes. The improved compressive strength due to the interfacial bond and formation of organic-inorganic composite in the microstructure is schematically shown in Fig. 16.

The compressive strength of the albumin, whey protein and SBI modified carbonated wollastonite pastes was increasingly higher at all protein concentrations and carbonation period. The increased compressive strength of these pastes is possibly due to the absence of cracks as shown in Fig. 13b, 13d, 13f and 13g, 13i, 13k and summarized in Table 2.

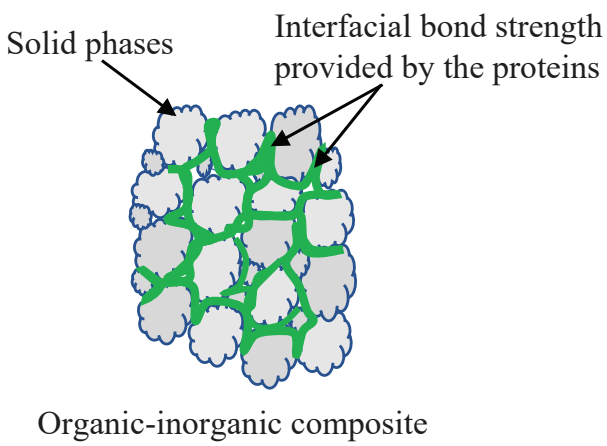

Fig. 16. The interfacial bond strength between solid phases in the microstructure provided by the proteins.

It was shown in section 3.1.3 that the proteins increased the flowability of the pastes; thus, it is expected that the proteins may have also enhanced the compressive strength of the carbonated wollastonite pastes by improving particle packing density and uniform distribution of reaction products. Although there are some differences between material properties, a similar scenario was reported by Zhu et al. [46] where they studied the effect of hydrophobic micelles on the workability, hydration process and microstructure of cement paste. Refinement of the pore structure of carbonated wollastonite pastes due to the addition of amino acids has been reported by Khan et al. [7].

It can be seen that carbonated wollastonite pastes modified with 0.25% concentration of the proteins showed higher compressive strength compared to the carbonated pastes modified with 1% protein concentration. This could be due to a lower total porosity as shown in Table 2. In addition, the self-aggregation effect when higher concentration of protein or polymer is used could reduce compressive strength [82]. The slightly lower $CaCO_3$ content revealed in Fig. 9 of the pastes modified with 1% protein concentration compared to the 0.25% protein modified pastes may be a factor too.

In order to evaluate the wet strength of the control and protein modified pastes, the carbonated wollastonite pastes with 1% protein concentration were submerged in water for 24 h. After the duration, the pastes were taken out of the water, wiped and their compressive strength measured. There was a reduction in the compressive strength of the albumin, CP and NFMP modified carbonated wollastonite pastes after submersion in water. The observed reduction in the compressive strength of these pastes could be caused by loss of interfacial strength in between carbonation products provided by protein adhesion. A reduction in adhesive strength of certain proteins has been observed in a prior investigation [26]. Baffoe and Ghahremaninezhad [26] reported a decreased adhesive strength in EICP treated ground hardened cement paste modified with NFMP and attributed the reduction to increased moisture content in the treated medium. It should be pointed out that the pastes with CP, NFMP and albumin showed cracks in the internal structure of the pastes. Thus, the water transport is expected to have been enhanced in these pastes and contributed to the lower interfacial strength provided by these proteins. Nonetheless, the pastes with SBI and whey protein did not show a reduction after being subjected to water submersion. This is related to the specific molecular structure of these proteins that endows them the ability to maintain their adhesion strength in a wet condition. In addition, the absence of cracks, smaller void porosity and size, and increased pore surface hydrophobicity induced by these two proteins as demonstrated in Fig. 5, hamper water transport into these pastes and reduce the contact between the proteins and water in the microstructure of these pastes. It can be seen that the compressive strength of the paste with albumin was still slightly higher

than that of the control after exposure to water submersion. The control paste did not show any changes in the compressive strength before and after exposure to water submersion as seen in Fig. 15.

4. Significance

The study signifies the benefits of using cost-effective and environmentally-friendly proteins in carbonated cured binders to advance green infrastructure materials. The incorporation of certain proteins exhibited great benefits in modifying microstructure to reduce cracking and improve mechanical performance.

5. Conclusions

In this study, the effect of 5 proteins with different molecular structures on the mineralization, microstructure and mechanical properties of carbonated wollastonite pastes was investigated. The findings from this study are as follows.

- The surface charge of the wollastonite particles was shown to increase with the addition of proteins due to the adsorption of negatively charged proteins onto the wollastonite particle surface. It is hypothesized that the proteins' moderate adsorption was primarily due to the electrostatic interaction between the negatively charged proteins and the negatively charged wollastonite particles via Ca^{2+} bridging. In addition, due to the presence of a variety of functional groups in the molecular structure of the proteins, other possible interactions including hydrogen bonds and hydrophobic bonds were suggested to contribute to the adsorption of some of the proteins onto the wollastonite surface.
- Higher flow values were observed in the fresh wollastonite paste with proteins compared to the paste without proteins and the increase in flow was shown to increase with increasing protein concentration. The reason for the increased flow was ascribed to the increased electrostatic repulsion between the protein-adsorbed wollastonite particles as evident in the zeta potential measurement, as well as ball bearing effect and formation of air bubbles due to the air entraining capacity of some of the proteins.
- In the paste with the proteins, the surface tension of the pore solution was shown to decrease while the water contact angle of the paste surface was shown to increase due to the presence of hydrophobic functional groups in the molecular structure of the proteins. The pore surface hydrophobization ability of the proteins was shown to have important impact on the phase formation and microstructure of the carbonated wollastonite pastes.
- While the SEM results revealed that calcite, ACC, and partially reacted wollastonite particles were the main reaction products in the carbonated pastes at both early and late ages, the results of the FTIR, TGA and XRD analysis revealed that in addition to the above-mentioned phases, other metastable phases including vaterite and aragonite were formed to a smaller extent, in the majority of the carbonated pastes with the proteins. This indicated that some proteins stabilized these metastable phases through the period of carbonation. It was also observed that the pastes with the proteins influenced the morphology by increasing the size of the calcite crystals.
- Some of the proteins resulted in a higher $CaCO_3$ content in the paste compared to the control paste. The reason for this increase is attributed to the hydrophobization of the pore structure, which delayed water loss and hence made free water available for the carbonation reaction to proceed.
- The micro-CT examination of the carbonated pastes revealed that the control, albumin, NFMP and CP carbonated pastes showed cracks. The reason for the crack formation in these pastes was attributed to increased drying shrinkage despite being cured in a chamber with a relative humidity of more than 95%. The obvious absence of cracks in the carbonated pastes with whey protein and SBI at 1% and 0.25% concentration, and reduced crack formation in the paste with albumin (0.25%) were attributed to the capillary pore surface hydrophobization in these pastes. Reduced water transport and evaporation and decreased capillary forces result from the pore surface hydrophobization effect of the proteins.
- Overall, the compressive strength of the carbonated pastes mixed with the proteins was shown to be higher than that of the control paste. Increased compressive strength was more pronounced in whey protein, SBI and albumin modified pastes especially at the 0.25% concentration. Absence of cracks, enhanced interfacial strength between carbonation products, and formation of inorganic-organic composite phases in the microstructure provided by these proteins were suggested to be the reasons for the enhanced compressive strength of some of the pastes mixed with proteins compared to the control paste.

Declaration of competing interest

The authors declare that they have no known competing financial interests or personal relationships that could have appeared to influence the work reported in this paper.

Data availability

Data will be made available on request.

Acknowledgements

This study was supported in part by the National Science Foundation under the CAREER award number 1846984 and the MRI award number 1920127. Any opinions, findings, and conclusions or recommendations expressed in this material are those of the author(s) and do not necessarily reflect the views of the National Science Foundation.

References

[1] E. Worrell, L. Price, N. Martin, C. Hendriks, L.O. Meida, Carbon dioxide emissions from the global cement industry, Annu. Rev. Energy Environ. 26 (2001) 303–329.
[2] A.M. Omer, Energy efficiency improvement utilising high technology: an assessment of energy use in industry, buildings development and the environment, Adv. Energy Res. 17 (2014) 39–75, https://doi.org/10.2139/ssrn.2403145.
[3] S.A. Bernal, J.L. Provis, B. Walkley, R. San Nicolas, J.D. Gehman, D.G. Brice, A. R. Kilcullen, P. Duxson, J.S.J. Van Deventer, Gel nanostructure in alkali-activated binders based on slag and fly ash, and effects of accelerated carbonation, Concr. Res. 53 (2013) 127–144, https://doi.org/10.1016/j.cemconres.2013.06.007.
[4] C. Bilim, O. Karahan, C.D. Atiş, S. İlkentapar, Effects of chemical admixtures and curing conditions on some properties of alkali-activated cementless slag mixtures, KSCE J. Civ. Eng. 19 (2015) 733–741, https://doi.org/10.1007/s12205-015-0629-0.
[5] Z.Y. Qu, Q. Yu, Y.D. Ji, F. Gauvin, I.K. Voets, Mitigating shrinkage of alkali activated slag with biofilm, Cement Concr. Res. 138 (2020), https://doi.org/10.1016/j.cemconres.2020.106234.
[6] H. Ye, A. Radlińska, Shrinkage mechanisms of alkali-activated slag, Cement Concr. Res. 88 (2016) 126–135, https://doi.org/10.1016/j.cemconres.2016.07.001.
[7] R.I. Khan, W. Ashraf, J. Olek, Amino acids as performance-controlling additives in carbonation-activated cementitious materials, Cement Concr. Res. 147 (2021), 106501, https://doi.org/10.1016/j.cemconres.2021.106501.
[8] B. Vafaei, K. Farzanian, A. Ghahremaninezhad, The influence of superabsorbent polymer on the properties of alkali-activated slag pastes, Construct. Build. Mater. 236 (2020), 117525, https://doi.org/10.1016/j.conbuildmat.2019.117525.
[9] J. Prabahar, B. Vafaei, E. Baffoe, A. Ghahremaninezhad, The effect of biochar on the properties of alkali-activated slag pastes, Constr. Mater. 2 (2021) 1–14, https://doi.org/10.3390/constrmater2010001.
[10] Y. Farnam, C. Villani, T. Washington, M. Spence, J. Jain, W. Jason Weiss, W. J. Weiss, Performance of carbonated calcium silicate based cement pastes and mortars exposed to NaCl and MgCl2 deicing salt, Construct. Build. Mater. 111 (2016) 63–71, https://doi.org/10.1016/j.conbuildmat.2016.02.098.
[11] W. Ashraf, J. Olek, N. Tian, Multiscale characterization of carbonated wollastonite paste and application of homogenization schemes to predict its effective elastic modulus, Cem. Concr. Compos. 72 (2016) 284–298, https://doi.org/10.1016/j.cemconcomp.2016.05.023.
[12] W. Ashraf, J. Olek, J. Jain, Microscopic features of non-hydraulic calcium silicate cement paste and mortar, Cement Concr. Res. 100 (2017) 361–372, https://doi.org/10.1016/j.cemconres.2017.07.001.

[13] W.J.J.J. Huijgen, G.J. Witkamp, R.N.J.J. Comans, Mechanisms of aqueous wollastonite carbonation as a possible CO2 sequestration process, Chem. Eng. Sci. 61 (2006) 4242–4251, https://doi.org/10.1016/j.ces.2006.01.048.
[14] J.M. Bukowski, R.L. Berger, Reactivity and strength development of CO2 activated non-hydraulic calcium silicates, Cement Concr. Res. 9 (1979) 57–68, https://doi.org/10.1016/0008-8846(79)90095-4.
[15] W. Seifritz, CO_2 disposal by means of silicates, Nature 345 (1990) 486.
[16] W. Ashraf, J. Olek, S. Sahu, Phase evolution and strength development during carbonation of low-lime calcium silicate cement (CSC), Construct. Build. Mater. 210 (2019) 473–482, https://doi.org/10.1016/j.conbuildmat.2019.03.038.
[17] W. Ashraf, J. Olek, H. Jeong, V. Atakan, Effects of high temperature on carbonated calcium silicate cement (csc) and ordinary portland cement (OPC) paste, in: Int. Conf. Durab. Concr. Struct. ICDCS 2016, 2016, pp. 1–7, https://doi.org/10.5703/1288284316153.
[18] P. De Silva, L. Bucea, D.R. Moorehead, V. Sirivivatnanon, Carbonate binders: reaction kinetics, strength and microstructure, Cem. Concr. Compos. 28 (2006) 613–620, https://doi.org/10.1016/j.cemconcomp.2006.03.004.
[19] D.R. Moorehead, Cementation by the carbonation of hydrated lime, Cement Concr. Res. 16 (1986) 700–708, https://doi.org/10.1016/0008-8846(86)90044-X.
[20] C. Briegel, H. Coelfen, J. Seto, Single amino acids as additives modulating CaCO3 mineralization, Adv. Top. Biominer. 33 (2012) E7–A85, https://doi.org/10.5772/39297.
[21] T.H.K.K. Nawarathna, K. Nakashima, T. Kawabe, W. Mwandira, K. Kurumisawa, S. Kawasaki, Artificial fusion protein to facilitate calcium carbonate mineralization on insoluble polysaccharide for efficient biocementation, Chem 9 (2021) 11493–11502, https://doi.org/10.1021/acssuschemeng.1c03730.
[22] I. Polowczyk, A. Bastrzyk, M. Fiedot, Protein-mediated precipitation of calcium carbonate, Materials 9 (2016) 1–16, https://doi.org/10.3390/ma9110944.
[23] H. Yang, W. Yao, L. Yang, X. Ma, H. Wang, F. Ye, K. Wong, The self-assembly of CaCO3 crystals in the presence of protein, J. Cryst. Growth 311 (2009) 2682–2688, https://doi.org/10.1016/j.jcrysgro.2009.02.049.
[24] Y.Y. Kim, J.D. Carloni, B. Demarchi, D. Sparks, D.G. Reid, M.E. Kunitake, C. C. Tang, M.J. Duer, C.L. Freeman, B. Pokroy, K. Penkman, J.H. Harding, L. A. Estroff, S.P. Baker, F.C. Meldrum, Tuning hardness in calcite by incorporation of amino acids, Nat. Mater. 15 (2016) 903–910, https://doi.org/10.1038/nmat4631.
[25] N.D.V. Raydan, L. Leroyer, B. Charrier, E. Robles, Recent advances on the development of protein-based adhesives for wood composite materials—a review, Molecules 26 (2021), https://doi.org/10.3390/molecules26247617.
[26] E. Baffoe, A. Ghahremaninezhad, The effect of biomolecules on enzyme-induced calcium carbonate precipitation in cementitious materials, Construct. Build. Mater. 345 (2022) 3, https://doi.org/10.1016/j.conbuildmat.2022.128323.
[27] T.V. Arriaga, Controlled and Tailored Denaturation and Aggregation of Whey Proteins Tatiana Vieira Arriaga Engenharia Biológica Júri, 2011. Thesis.
[28] M.D. Shoulders, R.T. Raines, Collagen structure and stability, Annu. Rev. Biochem. 78 (2009) 929–958, https://doi.org/10.1146/annurev.biochem.77.032207.120833.
[29] M. Singh, Structural interactions of globular proteins - bovine serum albumin, egg albumin, and lysozyme, in aqueous medium, elucidated with molar volumes, viscosities, energy functions, and IR spectra from 293.15 to 303.15 K, J. Appl. Polym. Sci. 103 (2007) 1420–1429, https://doi.org/10.1002/app.24626.
[30] N.S. Utay, D.M. Asmuth, S. Gharakhanian, M. Contreras, C.D. Warner, C.J. Detzel, Potential use of serum-derived bovine immunoglobulin/protein isolate for the management of COVID-19, Drug Dev. Res. 82 (2021) 873–879, https://doi.org/10.1002/ddr.21841.
[31] H. Bian, Colloidal Behavior of Casein Biopolymer in Alkaline Solution and its Application in Self-Levelling Underlayments (SLUs), Doctoral Dissertation, Technical University of Munich, 2012, https://mediatum.ub.tum.de/doc/1097342/file.pdf. (Accessed 15 April 2023).
[32] M.H. Abd El-Salam, S. El-Shibiny, Natural Biopolymers as Nanocarriers for Bioactive Ingredients Used in Food Industries, Encapsulations. 2016, 2016, pp. 793–829, https://doi.org/10.1016/b978-0-12-804307-3.00019-3.
[33] M.S.T. Masoule, E. Baffoe, A. Ghahremaninezhad, On the physicochemical properties and foaming characteristics of proteins in cement environment, Construct. Build. Mater. 366 (2023), 130204, https://doi.org/10.1016/j.conbuildmat.2022.130204.
[34] C.T. Lim, F. Lolli, J.D. Thomas, B. Kola, M. Korbonits, Measurement of AMP-activated protein kinase activity and expression in response to ghrelin, Methods Enzymol. 514 (2012) 271–287, https://doi.org/10.1016/B978-0-12-381272-8.00017-9.
[35] P.K. Smith, R.I. Krohn, G.T. Hermanson, A.K. Mallia, F.H. Gartner, M. D. Provenzano, E.K. Fujimoto, N.M. Goeke, B.J. Olson, D.C. Klenk, Measurement of protein using bicinchoninic acid, Anal. Biochem. 150 (1985) 76–85, https://doi.org/10.1016/0003-2697(85)90442-7.
[36] Z.H. Xue, S.X. Dai, B. Bin Hu, Z.L. Du, Effect of Langmuir monolayer of bovine serum albumin protein on the morphology of calcium carbonate, Mater. Sci. Eng. C 29 (2009) 1998–2002, https://doi.org/10.1016/j.msec.2009.03.016.
[37] E. Baffoe, A. Ghahremaninezhad, On the interaction between proteins and cracked cementitious surface, Construct. Build. Mater. 352 (2022) 2, https://doi.org/10.1016/j.conbuildmat.2022.128982.
[38] M.O. Kangal, G. Bulut, O. Guven, Physicochemical characterization of natural wollastonite and calcite, Minerals 10 (2020), https://doi.org/10.3390/min10030228.
[39] S. Chandra, J. Aavik, Influence of proteins on some properties of portland cement mortar, Int, J. Cem. Compos. 9 (1987) 91–94, https://doi.org/10.1016/0262-5075(87)90024-8.
[40] A.D. Nisbet, R.H. Saundry, A.J.G. Moir, L.A. Fothergill, J.E. Fothergill, The Complete amino-acid sequence of hen ovalbumin, Eur. J. Biochem. 115 (1981) 335–345, https://doi.org/10.1111/j.1432-1033.1981.tb05243.x.
[41] H. Bian, J. Plank, Effect of heat treatment on the dispersion performance of casein superplasticizer used in dry-mix mortar, Cement Concr. Res. 51 (2013) 1–5, https://doi.org/10.1016/j.cemconres.2013.04.004.
[42] P. Brzyski, Z. Suchorab, G. Łagód, The influence of casein protein admixture on pore size distribution and mechanical properties of lime-metakaolin paste, Buildings 11 (2021), https://doi.org/10.3390/buildings11110530.
[43] C. Zhang, X. Kong, J. Yu, D. Jansen, J. Pakusch, S. Wang, Correlation between the adsorption behavior of colloidal polymer particles and the yield stress of fresh cement pastes, Cement Concr. Res. 152 (2022), 106668, https://doi.org/10.1016/j.cemconres.2021.106668.
[44] Y. He, X. Zhang, R.D. Hooton, Y. Wang, Y. Kong, X. Wang, H. Wang, Influence of PCE on rheological and hydration performances of cement paste, J. Mater. Civ. Eng. 32 (2020), 04020002, https://doi.org/10.1061/(asce)mt.1943-5533.0002924.
[45] W.S. Chiang, E. Fratini, F. Ridi, S.H. Lim, Y.Q. Yeh, P. Baglioni, S.M. Choi, U. S. Jeng, S.H. Chen, Microstructural changes of globules in calcium-silicate-hydrate gels with and without additives determined by small-angle neutron and X-ray scattering, J. Colloid Interface Sci. 398 (2013) 67–73, https://doi.org/10.1016/j.jcis.2013.01.065.
[46] Y.Y. Zhu, J. Hu, Y.W. Ma, H.B. Xie, W.H. Guo, J.X. Wei, Q.J. Yu, The effect of micelles with random pH-sensitive/hydrophobic structure on the workability, hydration process and microstructure of cement paste, RSC Adv. 7 (2017) 17085–17094, https://doi.org/10.1039/c6ra26643f.
[47] M. Hashim, M. Tantray, Comparative study on the performance of protein and synthetic-based foaming agents used in foamed concrete, Case Stud. Constr. Mater. 14 (2021), e00524, https://doi.org/10.1016/j.cscm.2021.e00524.
[48] H. Bessaies-Bey, R. Baumann, M. Schmitz, M. Radler, N. Roussel, Effect of polyacrylamide on rheology of fresh cement pastes, Cement Concr. Res. 76 (2015) 98–106, https://doi.org/10.1016/j.cemconres.2015.05.012.
[49] Z. Lu, X. Kong, C. Zhang, F. Xing, Y. Zhang, Effect of colloidal polymers with different surface properties on the rheological property of fresh cement pastes, Colloids Surfaces A Physicochem. Eng. Asp. 520 (2017) 154–165, https://doi.org/10.1016/j.colsurfa.2017.01.067.
[50] G.J. Lesser, G.D. Rose, Hydrophobicity of amino acid subgroups in proteins, Proteins: Struct., Funct., Bioinf. 8 (1990) 6–13, https://doi.org/10.1002/prot.340080104.
[51] C. Nick Pace, J. Martin Scholtz, G.R. Grimsley, Forces stabilizing proteins, FEBS Lett. 588 (2014) 2177–2184, https://doi.org/10.1016/j.febslet.2014.05.006.
[52] J. Li, C. Wang, X. Li, Y. Su, Y. Yang, X. Yu, Effects of pH and NaCl on the physicochemical and interfacial properties of egg white/yolk, Food Biosci. 23 (2018) 115–120, https://doi.org/10.1016/j.fbio.2017.12.004.
[53] W. Huang, X. Sun, Adhesive properties of soy proteins modified by urea and guanidine hydrochloride, JAOCS, J. Am. Oil Chem. Soc. 77 (2000) 101–104, https://doi.org/10.1007/s11746-000-0016-6.
[54] S. Chandra, J. Aavik, Influence of black gram (natural organic material) addition as admixture in cement mortar and concrete, Cement Concr. Res. 13 (1983) 423–430, https://doi.org/10.1016/0008-8846(83)90043-1.
[55] A. Kato, S. Nakai, Hydrophobicity determined by a fluorescence probe method and its correlation with surface properties of proteins, Biochim. Biophys. Acta 624 (1980) 13–20, https://doi.org/10.1016/0005-2795(80)90220-2.
[56] H. Xiao, L. Huang, W. Zhang, Z. Yin, Damage of proteins at the air/water interface: surface tension characterizes globulin interface stability, Int. J. Pharm. 584 (2020), 119445, https://doi.org/10.1016/j.ijpharm.2020.119445.
[57] W. Ashraf, J. Olek, Carbonation behavior of hydraulic and non-hydraulic calcium silicates: potential of utilizing low-lime calcium silicates in cement-based materials, J. Mater. Sci. 51 (2016) 6173–6191, https://doi.org/10.1007/s10853-016-9909-4.
[58] Y. Ping, R.J. Kirkpatrick, P. Brent, P.F. McMillan, X. Cong, Structure of calcium silicate hydrate (C-S-H): near-, mid-, and far-infrared spectroscopy, J. Am. Ceram. Soc. 82 (1999) 742–748, https://doi.org/10.1111/j.1151-2916.1999.tb01826.x.
[59] A. A, L.B. Fleming, Infrared spectra of amorphous and crystalline calcium carbonate, Acta Chem. Scand. 45 (1991) 1018–1024.
[60] T.L. Hughes, C.M. Methven, T.G.J. Jones, S.E. Pelham, P. Fletcher, C. Hall, Determining cement composition by Fourier transform infrared spectroscopy, Adv. Cement Base Mater. 2 (1995) 91–104, https://doi.org/10.1016/1065-7355(94)00031-X.
[61] C.E. Weir, E.R. Lippincott, Infrared studies of aragonite, calcite, and vaterite type structures in the borates, carbonates, and nitrates, J. Res. Natl. Bur. Stand. Sect. A Phys. Chem. 65A (1961) 173, https://doi.org/10.6028/jres.065a.021.
[62] S.A. Bernal, J.L. Provis, D.G. Brice, A. Kilcullen, P. Duxson, J.S.J. Van Deventer, Accelerated carbonation testing of alkali-activated binders significantly underestimates service life: the role of pore solution chemistry, Cement Concr. Res. 42 (2012) 1317–1326, https://doi.org/10.1016/j.cemconres.2012.07.002.
[63] W. Ashraf, J. Olek, Elucidating the accelerated carbonation products of calcium silicates using multi-technique approach, J. CO2 Util. 23 (2018) 61–74, https://doi.org/10.1016/j.jcou.2017.11.003.
[64] Y. Min, Q. Li, M. Voltolini, T. Kneafsey, Y.S. Jun, Wollastonite carbonation in water-bearing supercritical CO2: effects of particle size, Environ. Sci. Technol. 51 (2017) 13044–13053, https://doi.org/10.1021/acs.est.7b04475.
[65] S. Zdenek, Carbonization of porous concrete and its main binding components, Cement Concr. Res. 1 (1971) 645–662.

[66] D.B. DeOliveira, R.A. Laursen, Control of calcite crystal morphology by a peptide designed to bind to a specific surface, J, Am. Chem. 119 (1997) 10627–10631, https://doi.org/10.1021/ja972270w.
[67] G. Jain, M. Pendola, Y.C. Huang, D. Gebauer, J.S. Evans, A model sea Urchin Spicule matrix protein, rSpSM50, is a hydrogelator that modifies and organizes the mineralization process, Biochemistry 56 (2017) 2663–2675, https://doi.org/10.1021/acs.biochem.7b00083.
[68] Y. Min, Y.S. Jun, Wollastonite carbonation in water-bearing supercritical CO2: effects of water saturation conditions, temperature, and pressure, Chem. Geol. 483 (2018) 239–246, https://doi.org/10.1016/j.chemgeo.2018.01.012.
[69] M. Thiery, G. Villain, P. Dangla, G. Platret, Investigation of the carbonation front shape on cementitious materials: effects of the chemical kinetics, Cement Concr. Res. 37 (2007) 1047–1058, https://doi.org/10.1016/j.cemconres.2007.04.002.
[70] W. Ashraf, J. Olek, Carbonation activated binders from pure calcium silicates: reaction kinetics and performance controlling factors, Cem. Concr. Compos. 93 (2018) 85–98, https://doi.org/10.1016/j.cemconcomp.2018.07.004.
[71] J.M. Walker, B. Marzec, F. Nudelman, Solid-state transformation of amorphous calcium carbonate to aragonite captured by cryoTEM, Angew, Chemie - Int. 56 (2017) 11740–11743, https://doi.org/10.1002/anie.201703158.
[72] V.T. Ngala, C.L. Page, Effects of carbonation on pore structure and diffusional properties of hydrated cement pastes, Cement Concr. Res. 27 (1997) 995–1007.
[73] T. Chen, X. Gao, Effect of carbonation curing regime on strength and microstructure of Portland cement paste, J. CO2 Util. 34 (2019) 74–86, https://doi.org/10.1016/j.jcou.2019.05.034.
[74] A. Morandeau, M. Thiéry, P. Dangla, Investigation of the carbonation mechanism of CH and C-S-H in terms of kinetics, microstructure changes and moisture properties, Cem, Concr. Res. 56 (2014) 153–170, https://doi.org/10.1016/j.cemconres.2013.11.015.
[75] L. Du, K.J. Folliard, Mechanisms of air entrainment in concrete, Cement Concr. Res. 35 (2005) 1463–1471, https://doi.org/10.1016/j.cemconres.2004.07.026.
[76] A.H. Martin, K. Grolle, M.A. Bos, M.A. Cohen Stuart, T. Van Vliet, Network forming properties of various proteins adsorbed at the air/water interface in relation to foam stability, J. Colloid Interface Sci. 254 (2002) 175–183, https://doi.org/10.1006/jcis.2002.8592.
[77] E. Dickinson, Milk protein interfacial layers and the relationship to emulsion stability and rheology, Colloids Surf. B Biointerfaces 20 (2001) 197–210, https://doi.org/10.1016/S0927-7765(00)00204-6.
[78] A. Saint-Jalmes, M.L. Peugeot, H. Ferraz, D. Langevin, Differences between protein and surfactant foams: microscopic properties, stability and coarsening, Colloids Surfaces A Physicochem. Eng. Asp. 263 (2005) 219–225, https://doi.org/10.1016/j.colsurfa.2005.02.002.
[79] J. Wang, A.V. Nguyen, S. Farrokhpay, A critical review of the growth, drainage and collapse of foams, Adv. Colloid Interface Sci. 228 (2016) 55–70, https://doi.org/10.1016/j.cis.2015.11.009.
[80] C. Stubenrauch, R. Miller, Stability of foam films and surface rheology: an oscillating bubble study at low frequencies, J. Phys. Chem. B 108 (2004) 6412–6421, https://doi.org/10.1021/JP049694E.
[81] L.E. Tunstall, M.T. Ley, G.W. Scherer, Air entraining admixtures: mechanisms, evaluations, and interactions, Cement Concr. Res. 150 (2021), 106557, https://doi.org/10.1016/j.cemconres.2021.106557.
[82] S.J. Choi, S.H. Bae, J.I. Lee, E.J. Bang, H.M. Ko, Strength, carbonation resistance, and chloride-ion penetrability of cement mortars containing catechol-functionalized chitosan polymer, Materials 14 (2021) 6395, https://doi.org/10.3390/MA14216395.
[83] B. Cantaert, D. Kuo, S. Matsumura, T. Nishimura, T. Sakamoto, T. Kato, Use of amorphous calcium carbonate for the design of new materials, ChemPlusChem 82 (2017) 107–120, https://doi.org/10.1002/cplu.201600457.